Eur. Phys. J. C 47, 481–505 (2006)
Digital Object Identifier (DOI) 10.1140/epjc/s2006-02541-7

THE EUROPEAN PHYSICAL JOURNAL C

Phenomenological aspects of heterotic orbifold models at one loop

P. Binétruy[1], A. Birkedal-Hansen[2], Y. Mambrini[1], B.D. Nelson[3,a]

[1] Laboratoire de Physique Théorique, Université Paris-Sud, 91405 Orsay, France
[2] Department of Physics and Theoretical Physics Group, Lawrence Berkeley Laboratory, University of California, Berkeley, CA 94720, USA
[3] Michigan Center for Theoretical Physics, Randall Laboratory, University of Michigan, Ann Arbor, MI 48109, USA

Received: 18 January 2005 / Revised version: 26 April 2005 /
Published online: 24 May 2006 –

Abstract. We provide a detailed study of the phenomenology of orbifold compactifications of the heterotic string within the context of supergravity effective theories. Our investigation focuses on those models where the soft Lagrangian is dominated by loop contributions to the various soft supersymmetry breaking parameters. Such models typically predict non-universal soft masses and are thus significantly different from minimal supergravity and other universal models. We consider the pattern of masses that are governed by these soft terms and investigate the implications of certain indirect constraints on supersymmetric models, such as flavor-changing neutral currents, the anomalous magnetic moment of the muon and the density of thermal relic neutralinos. We also comment on the possible discovery of these models at the LHC. These string-motivated models show a novel behavior that interpolates between the phenomenology of unified supergravity models and models dominated by the superconformal anomaly.

PACS. 11.25.Wx; 12.60.Jv; 04.65.+e

1 Introduction

The recent interest in models where supersymmetry breaking is transmitted from a hidden sector to our observable world via the superconformal anomaly [1–3] has served as a reminder that there are occasions where working at one-loop order is more than a theoretical luxury, but an absolute necessity if one is to understand even the gross features of some models. Recently, the complete one loop supergravity correction to soft supersymmetry breaking terms was obtained [4, 5], a subset of which are the aforementioned "anomaly-mediated" terms. The broad features of these corrections, in particular for gaugino masses, was studied in a heterotic string context in [6]. In the current work, we wish to study in greater detail the low energy phenomenology of models based on orbifold compactifications of the weakly-coupled heterotic string in which these loop corrections are significant. To that extent we will choose two "laboratories" in which tree-level soft supersymmetry breaking terms are either absent or greatly suppressed.

Our first example will involve an observable sector in which the matter fields are assumed to be from the untwisted sector of the orbifold compactification. In the event that supersymmetry breaking is transmitted by the compactification moduli T^α, whose vacuum expectation values determine the size of the compact manifold, this model will exhibit a no-scale pattern of soft terms with vanishing soft supersymmetry breaking terms at tree-level. Clearly, the phenomenology of such models will depend critically on the form of the loop induced soft terms. Indeed, the "sequestered sector" models considered in [2] were of just such a form.

In our second example we will switch our focus to cases in which it is the dilaton field S whose vacuum expectation value determines the magnitude of the (unified) coupling constant $g_{\rm STR}$ at the string scale that participates exclusively in supersymmetry breaking. We will work in the context of models in which string nonperturbative corrections to the Kähler potential act to stabilize the dilaton in the presence of gaugino condensation [7, 8]. Such theories predict a suppression of dilaton contributions to soft terms relative to those of the supergravity auxiliary field — thereby suppressing tree-level contributions to supersymmetry breaking relative to certain loop contributions.

After describing our framework and introducing both the tree-level and one loop soft supersymmetry breaking terms in Sect. 2, we introduce the parameter space for our two broad classes of models in Sect. 3. The subsequent section describes the analysis tools that we employ and the types of low-energy phenomena that we will study before describing the implications of low-energy experimental

[a] e-mail: bnelson@sage.hep.upenn.edu
Present address: Department of Physics & Astronomy, University of Pennsylvania, Philadelphia, PA 19104, USA

constraints on each of our models and possible particle discovery at the LHC in Sect. 5.

In general, we find that these examples have a phenomenology that combines the features of minimal supergravity (mSUGRA) models with those of anomaly-mediated models. Parameters related to the orbifold compactification and the stabilization of string moduli interpolate between these regimes. These models are thus important for preparing for forthcoming LHC data, as the challenges of the anomaly-mediated paradigm for hadron colliders have mostly been probed only in the "minimal" paradigm [9]. Our study is also a useful complement to other recent studies of string-based phenomenology inspired by other constructions [10, 11]. Current observations and particle mass limits from collider experiments already shed light on the nature of moduli stabilization. Our results suggest that future discoveries of superpartners will be likely to provide strong evidence in favor of one stabilization mechanism or another in the context of weakly-coupled heterotic string models.

2 The structure of heterotic orbifold models at one loop

We work in a framework in which the chiral superfields Z^M can be divided into two classes: observable sector superfields, denoted Z^i, charged under the observable sector gauge symmetries; and hidden sector superfields, denoted Z^n. Since our interest here is primarily on broad issues of phenomenology, the hidden sector fields that we will consider are the dilaton S in the chiral multiplet formulation and the three diagonal Kähler moduli T^α.

In the orbifold compactifications that we study here, the tree-level Kähler potential for the moduli and the matter superfields is known. For the moduli sector, we have

$$K(S,\overline{S};T^\alpha,\overline{T}^\alpha) = k(S+\bar{S}) - \sum_{\alpha=1}^{3} \ln\left(T^\alpha+\overline{T}^\alpha\right) \,, \quad (1)$$

where we prefer to leave the form of the dilaton Kähler potential k unspecified at this point. Its precise form depends on how one stabilizes the dilaton. We will return to this issue when we discuss the dilaton-dominated scenario in Sect. 3.2. As for the observable sector matter fields Z^i with modular weights n_i^α associated with each of the three T^α, we assume a diagonal Kähler metric given by

$$K_{i\bar{j}} = \kappa_i(Z^n)\delta_{ij} + O(|Z^i|^2) \,, \quad (2)$$

with

$$\kappa_i(Z^n) = \prod_\alpha (T^\alpha+\overline{T}^\alpha)^{n_i^\alpha} \,. \quad (3)$$

In the interests of simplicity, we assume that the three Kähler moduli T^α can be treated as equivalent, so that

$$K(S,\overline{S};T,\overline{T}) = k(S+\overline{S}) - 3\ln(T+\overline{T}), \quad \kappa_i = (T+\overline{T})^{n_i} \,, \quad (4)$$

where $n_i = \sum_\alpha n_i^\alpha$.

The tree-level gauge kinetic functions $f_a(Z^n)$, one for each gauge group $\mathcal{G}_a$, are given in the weak coupling regime by

$$f_a^0(Z^n) = S \,. \quad (5)$$

Their vacuum expectation values give the associated gauge couplings $\langle \mathrm{Re} f_a\rangle = 1/g_a^2$. To (5) will be added certain string threshold corrections when we exhibit the one loop soft supersymmetry breaking terms below.

The scalar potential, written in terms of auxiliary fields, is given by the expression[1]

$$V = K_{I\overline{J}} F^I \overline{F}^{\bar{J}} - \frac{1}{3} M\overline{M} \,, \quad (6)$$

with $K_{I\overline{J}} = \partial^2 K/\partial Z^I \partial \overline{Z}^{\bar{J}}$ being the Kähler metric. The fields F^I in (6) are the auxiliary fields associated with the chiral superfields Z^I, while the field M is the auxiliary field of the supergravity multiplet. Solving the equations of motion for these auxiliary fields yields

$$F^M = -e^{K/2} K^{M\overline{N}} \left(\overline{W}_{\overline{N}} + K_{\overline{N}}\overline{W}\right) \,, \quad (7)$$

$$\overline{M} = -3e^{K/2}\overline{W} \,, \quad (8)$$

with $K^{M\overline{N}}$ being the inverse of the Kähler metric. Note that these expressions are given in terms of reduced Planck mass units where we have set $M_{\mathrm{PL}}/\sqrt{8\pi} = 1$. The supergravity auxiliary field is related to the gravitino mass by

$$M_{3/2} = -\frac{1}{3}\left\langle \overline{M}\right\rangle = \left\langle e^{K/2}\overline{W}\right\rangle \,. \quad (9)$$

We adopt the ansatz of Brignole et al. [12] in which one assumes that the communication of supersymmetry breaking from the hidden sector to the observable sector occurs through the agency of one of the moduli — in this case either the dilaton S or the (universal) Kähler modulus T — by the presence of a non-vanishing vacuum expectation value of their auxiliary fields F^S or F^T. In principle, both types of moduli could participate in supersymmetry breaking, and so one typically introduces a "Goldstino angle" θ to parameterize the degree to which one sector or the other feels the supersymmetry breaking. While this is a common practice, all known explicit models of moduli stabilization in the heterotic string context predict that this "angle" will be some integer multiple of $\pi/2$; that is, only one of the two classes of moduli participates in supersymmetry breaking.

If these are the only sectors with non-vanishing auxiliary fields in the vacuum, then the further requirement that the overall vacuum energy at the minimum of the potential (6) be zero allows us to immediately identify (up to phases, which we set to zero in what follows)

$$F^S = -\frac{1}{\sqrt{3}}\overline{M} k_{s\bar{s}}^{-1/2}\sin\theta = \sqrt{3} M_{3/2} k_{s\bar{s}}^{-1/2}\sin\theta \,, \quad (10)$$

$$F^T = -\frac{1}{\sqrt{3}}\overline{M} K_{t\bar{t}}^{-1/2}\cos\theta = \sqrt{3} M_{3/2} K_{t\bar{t}}^{-1/2}\cos\theta, \quad (11)$$

where the last equality holds for the vacuum expectation values, using (9) above. We should note that the condition

[1] We will assume vanishing D-terms in what follows.

of vanishing vacuum energy is a necessary one to employ the above parameterization. In this work, we will avoid discussing specific models of dynamical supersymmetry breaking and moduli stabilization, but any such model must include some mechanism for engineering a vanishing vacuum energy in order to make contact with the results presented here.

2.1 Modular invariance and tree-level supersymmetry breaking terms

The soft supersymmetry breaking terms in string-derived supergravity depend on the moduli through the observable sector superpotential and this, in turn, is determined by insisting on modular invariance of the low-energy effective Lagrangian. The diagonal modular transformations

$$T \to \frac{aT - \mathrm{i}b}{\mathrm{i}cT + d}, \quad ad - bc = 1, \quad a, b, c, d \in Z \tag{12}$$

leave the classical effective supergravity theory invariant, though at the quantum level these transformations are anomalous [13–16]. This anomaly is cancelled in the effective theory by the presence of a universal Green–Schwarz counterterm and model-dependent string threshold corrections [17, 18], which we describe below.

A matter field Z^i of modular weight n_i transforms under (12) as

$$Z^i \to (\mathrm{i}cT + d)^{n_i} Z^i \,, \tag{13}$$

while the Kähler potential of (4) undergoes a Kähler transformation $K \to K + 3(F + \overline{F})$, with $F = \ln(\mathrm{i}cT + d)$, under (12). Therefore, the classical symmetry will be preserved provided the superpotential transforms as [19]

$$W \to W\,(\mathrm{i}cT + d)^{-3} \,. \tag{14}$$

To ensure this transformation property, the superpotential of string-derived models has a moduli dependence of the form

$$W_{ijk} = w_{ijk}\,[\eta(T)]^{-2(3+n_i+n_j+n_k)} \,, \tag{15}$$

where $W_{ijk} = \partial^3 W(Z^N)/\partial Z^i \partial Z^j \partial Z^k$. The function $\eta(T)$ is the classical Dedekind eta function

$$\eta(T) = e^{-\pi T/12} \prod_{n=1}^{\infty} (1 - e^{-2\pi n T}) \tag{16}$$

and it has a well-defined transformation under (12) given by

$$\eta(T) \to (\mathrm{i}cT + d)^{1/2}\, \eta(T) \,. \tag{17}$$

We will also have to introduce the modified Eisenstein function

$$G_2\,(t, \bar{t}\,) \equiv 2\zeta(t) + \frac{1}{t + \bar{t}}, \quad \text{where } \zeta(T) = \frac{1}{\eta(T)} \frac{\mathrm{d}\eta(T)}{\mathrm{d}T} \,, \tag{18}$$

which vanishes at the self-dual points $t = 1$ and $t = e^{\mathrm{i}\pi/6}$.

We are now in a position to give the tree-level soft supersymmetry breaking terms. The tree-level gaugino mass for canonically normalized gaugino fields is simply

$$M_a^0 = \frac{g_a^2}{2} F^n \partial_n f_a^0 \,. \tag{19}$$

We define our trilinear A-terms and scalar masses for canonically normalized fields by

$$\begin{aligned} V_A &= \frac{1}{6} \sum_{ijk} A_{ijk} e^{K/2} W_{ijk} z^i z^j z^k + \text{ h.c.} \\ &= \frac{1}{6} \sum_{ijk} A_{ijk} e^{K/2} W_{ijk} \frac{\hat{z}^i \hat{z}^j \hat{z}^k}{\sqrt{\kappa_i \kappa_j \kappa_k}} + \text{ h.c.} \,, \end{aligned} \tag{20}$$

where $\hat{z}^i = \kappa_i^{1/2} z^i$ is a normalized scalar field, and by

$$V_M = \sum_i M_i^2 \kappa_i |z^i|^2 = \sum_i M_i^2 |\hat{z}^i|^2 \,. \tag{21}$$

With these conventions our tree-level expressions are

$$A_{ijk}^0 = \left\langle F^n \partial_n \ln(\kappa_i \kappa_j \kappa_k e^{-K}/W_{ijk}) \right\rangle \,. \tag{22}$$

$$(M_i^0)^2 = \left\langle \frac{M\overline{M}}{9} - F^n \overline{F}^{\bar{m}} \partial_n \partial_{\bar{m}} \ln \kappa_i \right\rangle \,. \tag{23}$$

If we specialize now to the case of (10) and (11) with moduli dependence given by (4), (5) and (15), then the tree-level gaugino masses (19), A-terms (22) and scalar masses (23) become

$$\begin{aligned} M_a^0 &= \frac{g_a^2}{2} F^S \\ A_{ijk}^0 &= (3 + n_i + n_j + n_k) G_2\,(t, \bar{t}\,)\, F^T - k_S F^S \\ \left(M_i^0\right)^2 &= \frac{M\overline{M}}{9} + n_i \frac{|F^T|^2}{(t + \bar{t}\,)^2} \,. \end{aligned} \tag{24}$$

The expressions in (24) are to be understood as vacuum values, though we will drop the cumbersome brackets $\langle \ldots \rangle$ from here onwards.

These tree-level soft terms have been studied extensively in the past and we wish to understand what impact the less-studied loop corrections can have on the phenomenology of orbifold models. We can now appreciate the importance of the two cases that we intend to study in Sects. 3.1 and 3.2. In the case where the modular weights of the observable sector are universally $n_i = -1$, as would be the case for the untwisted sector of orbifold compactifications, from (15) it is clear that the moduli do not couple to the observable sector through the superpotential and we have a true no-scale model. Indeed, substituting (11) into (24), we find that if the dilaton does not participate in supersymmetry breaking all ($\theta = 0$) tree-level soft terms are precisely zero in such a case. This is the situation that we will investigate in Sect. 3.1.

Alternatively, if the dilaton is the primary source of supersymmetry breaking in the observable sector, loop-level corrections to at least the trilinear A-terms and gaugino

masses will continue to be important provided that the magnitude of F^S is suppressed relative to that of M, as it is in models where nonperturbative corrections to the Kähler potential are used to stabilize the dilaton [20]. In such a scenario, the modular weights of the matter fields are irrelevant at the tree-level, so we will continue to assume $n_i = -1$ for the sake of convenience when we investigate these models in Sect. 3.2. We thus need to turn our attention to the study of soft supersymmetry breaking at one loop.

2.2 General one loop corrections to soft supersymmetry breaking

In this section, we aim to provide sufficient background to justify the form of the one loop soft term expressions that are our goal, as well as to explain some notation that we will need for our phenomenological analysis. For more complete explanations of what is contained in this section, including expressions with arbitrary modular weights and three independent Kähler moduli, the reader should consult the precursor to this work [6].

We begin with gaugino masses that can be understood as a sum of loop-induced contributions from the field theory point of view, and terms that can be thought of as one loop stringy corrections. The field theory loop contribution can be derived completely from the superconformal anomaly and is given by [4, 21]

$$M_a^1|_{\rm an} = \frac{g_a^2(\mu)}{2}\left[\frac{2b_a}{3}\overline{M} - \frac{1}{8\pi^2}\left(C_a - \sum_i C_a^i\right) \times F^n K_n - \frac{1}{4\pi^2}\sum_i C_a^i F^n \partial_n \ln \kappa_i\right], \quad (25)$$

where C_a, C_a^i are the quadratic Casimir operators for the gauge group $\mathcal{G}_a$ in the adjoint representation and in the representation of Z^i, respectively, and b_a is the beta-function coefficient for the group $\mathcal{G}_a$:

$$b_a = \frac{1}{16\pi^2}\left(3C_a - \sum_i C_a^i\right). \quad (26)$$

As mentioned in the previous section, one expects modular anomaly cancellation to occur through a universal Green–Schwarz counterterm with group-independent coefficient $\delta_{\rm GS}$. Such a term can be thought of as a loop correction that contributes to gaugino masses in the form

$$M_a^1|_{\rm GS} = \frac{g_a^2(\mu)}{2}\frac{2F^T}{(t+\bar{t})}\frac{\delta_{\rm GS}}{16\pi^2}. \quad (27)$$

In addition, string threshold corrections generally appear in the effective theory, which may be interpreted as one loop corrections to the gauge kinetic functions of the form

$$f_a^1(Z^n) = \ln \eta^2(T)\left[\frac{\delta_{\rm GS}}{16\pi^2} + b_a\right], \quad (28)$$

which generate loop contributions to gaugino masses given by

$$M_a^1|_{\rm th} = \frac{g_a^2(\mu)}{2}\left[\frac{\delta_{\rm GS}}{16\pi^2} + b_a\right] 4\zeta(t) F^T. \quad (29)$$

Putting together the tree-level gaugino mass with the loop contributions (25), (27) and (29) gives

$$M_a = \frac{g_a^2(\mu)}{2}\left\{2\left[\frac{\delta_{\rm GS}}{16\pi^2} + b_a\right] G_2(t,\bar{t})\, F^T + \frac{2}{3} b_a \overline{M} + [1 - 2b_a' k_s]\, F^S\right\}, \quad (30)$$

where we have defined the quantity

$$b_a' = \frac{1}{16\pi^2}\left(C_a - \sum_i C_a^i\right). \quad (31)$$

To understand the form of the one-loop A-terms and scalar masses it is necessary to describe how field theory loops are regulated in supergravity, seen as an effective theory of strings. The regulation of matter and Yang–Mills loop contributions to the matter wave function renormalization requires the introduction of Pauli–Villars chiral superfields $\Phi^A = \Phi^i$, $\widehat{\Phi}^i$ and Φ^a, which transform according to the chiral matter, anti-chiral matter and adjoint representations of the gauge group and have signatures $\eta_A = -1, +1, +1,$, respectively. These fields are coupled to the light fields Z^i through the superpotential

$$W(\Phi^A, Z^i) = \frac{1}{2} W_{ij}(Z^k)\Phi^i\Phi^j + \sqrt{2}\Phi^a \widehat{\Phi}_i (T_a Z)^i + \cdots, \quad (32)$$

where T_a is a generator of the gauge group, and their Kähler potential takes the schematic form

$$K_{\rm PV} = \sum_A \kappa_A^{\Phi}(Z^N)|\Phi^A|^2, \quad (33)$$

where the functions κ_A are a priori functions of the hidden sector (moduli) fields. These regulator fields must be introduced in such a way as to cancel the quadratic divergences of the light field loops — and thus their Kähler potential is determined relative to that of the fields that they regulate.

The PV mass for each superfield Φ^A is generated by coupling it to another field $\Pi^A = (\Pi^i, \widehat{\Pi}^i, \Pi^a)$ in the representation of the gauge group conjugate to that of Φ^A through a superpotential term

$$W_m = \sum_A \mu_A(Z^N)\Phi^A\Pi^A, \quad (34)$$

where $\mu_A(Z^N)$ can in general be a holomorphic function of the light superfields. There is no constraint on the Kähler potential for the fields Π^A as there was for that of the Φ^A. However, if we demand that our regularization preserve modular invariance then we can determine the moduli dependence of the regulator fields Φ^A

$$\begin{cases} \Phi^i: & \kappa_i^{\Phi} = \kappa_i = (T+\overline{T})^{n_i}, \\ \widehat{\Phi}^i: & \hat{\kappa}_i^{\Phi} = \kappa_i^{-1}, \\ \Phi^a: & \kappa_a^{\Phi} = g_a^{-2} e^K = g_a^{-2} e^k (T+\overline{T})^{-3}, \end{cases} \quad (35)$$

and we can determine the moduli dependence of the supersymmetric mass $\mu_A(Z^N)$ in (34)

$$\mu_A(Z^N) = \mu_A(S)\,[\eta(T)]^{-2(3+n_A+q_A)}\ , \tag{36}$$

with n_A and q_A being the modular weights of the fields Φ^A and Π^A, respectively. Furthermore, we can postulate the form of the moduli dependence of κ_A for the mass-generating fields

$$\Pi^A: \quad \kappa_A^{\Pi} = h_A(S+\overline{S})(T+\overline{T})^{q_A}\ . \tag{37}$$

So at this point the dilaton dependence in the superpotential term (34) and the functions h_A, as well as the modular weights q_A of the fields Π^A, are new free parameters of the theory introduced at one loop as a consequence of how the theory is regulated. Given (34), we can extract the Pauli–Villars masses that appear as regulator masses in the logarithms at one loop

$$m_A^2 = e^K \left(\kappa_A^{\Phi}\right)^{-1/2} \left(\kappa_A^{\Pi}\right)^{-1/2} |\mu_A|^2\ , \tag{38}$$

with $m_A = (m_i, \hat{m}_i, m_a)$ being the masses of the regulator fields $\Phi^i, \widehat{\Phi}^i, \Phi^a$, respectively.

In terms of these regulator masses, the complete one loop correction to the trilinear A-terms and scalar masses in a general supergravity theory was given in [5]. In this survey we will simplify the expressions and reduce the parameter space by making some reasonable assumptions. Let us first assume that the functions $\mu_A(Z^N)$ that appear in (34) and (38) are proportional to one overall Pauli–Villars scale $\mu_{\rm PV}$, so that $\hat{\mu}_i = \mu_a = \mu_i \equiv \mu_{\rm PV}$. This scale is presumed to represent some fundamental scale in the underlying string theory. Let us further assume that there is no dilaton dependence of the PV masses so that $h_A(S+\overline{S})$ is trivial and $\mu_{\rm PV}$ is constant. With these simplifications the complete trilinear A-term at one loop is given by

$$\begin{aligned} A_{ijk} = {} & \frac{1}{3}A^0_{ijk} - \frac{1}{3}\gamma_i\overline{M} - G_2\,(t,\bar{t})\,F^T \\ & \times \left(\sum_a \gamma_i^a p_{ia} + \sum_{lm}\gamma_i^{lm}p_{lm}\right) - \ln[(t+\bar{t})|\eta(t)|^4] \\ & \times \left(2\sum_a \gamma_i^a\ p_{ia}M_a^0 + \sum_{lm}\gamma_i^{lm}p_{lm}A^0_{ilm}\right) \\ & + 2\sum_a \gamma_i^a M_a^0 \ln\left(\mu^2_{\rm PV}/\mu_R^2\right) \\ & + \sum_{lm}\gamma_i^{lm}A^0_{ilm}\ln\left(\mu^2_{\rm PV}/\mu_R^2\right) + \text{cyclic}(ijk)\,, \end{aligned} \tag{39}$$

where we have defined the following combinations of modular weights from the Pauli–Villars sector

$$\begin{aligned} p_{ij} &= 3 + \frac{1}{2}\,(n_i + n_j + q_i + q_j)\,, \\ p_{ia} &= \frac{1}{2}\,(3 + q_a + \hat{q}_i - n_i)\ , \end{aligned} \tag{40}$$

which we will refer to as "regularization weights" in reference to their origin from the PV sector of the theory.[2]

In (39) M_a^0 and A^0_{ilm} are the tree-level gaugino masses and A-terms given in (24) and the parameters γ determine the chiral multiplet wave function renormalization

$$\gamma_i^j = \frac{1}{32\pi^2}\left[4\delta_i^j\sum_a g_a^2(T_a^2)_i^i - e^K\sum_{kl}W_{ikl}\overline{W}^{jkl}\right]\ . \tag{41}$$

We have implicitly made the approximation that generational mixing is unimportant and can be neglected in (39), and this motivates the definitions

$$\begin{aligned} &\gamma_i^j \approx \gamma_i\delta_i^j, \quad \gamma_i = \sum_{jk}\gamma_i^{jk} + \sum_a \gamma_i^a\,, \\ &\gamma_i^a = \frac{g_a^2}{8\pi^2}(T_a^2)_i^i, \quad \gamma_i^{jk} = -\frac{e^K}{32\pi^2}\frac{|W_{ijk}|^2}{\kappa_i\kappa_j\kappa_k}\,. \end{aligned} \tag{42}$$

The scalar masses are obtained similarly and take the form

$$\begin{aligned} (M_i)^2 = {} & (M_i^0)^2 + \gamma_i\frac{M\overline{M}}{9} \\ & - \frac{|F^T|^2}{(t+\bar{t})^2}\left(\sum_a \gamma_i^a p_{ai} + \sum_{jk}\gamma_i^{jk}p_{jk}\right) \\ & + \left\{F^T G_2\,(t,\bar{t})\left(\sum_a \gamma_i^a p_{ia}M_a^0 + \frac{1}{2}\sum_{jk}\gamma_i^{jk}p_{jk}A^0_{jk}\right)\right. \\ & \left. + \frac{M}{3}\left[\sum_a \gamma_i^a M_a^0 + \frac{1}{2}\sum_{jk}\gamma_i^{jk}A^0_{ijk}\right] + \text{ h.c.}\ \right\} \\ & - \ln\left[(t+\bar{t})|\eta(t)|^4\right]\left\{\sum_a \gamma_i^a\ p_{ia}\left[3(M_a^0)^2 - (M_i^0)^2\right]\right. \\ & \left. + \sum_{jk}\gamma_i^{jk}p_{jk}\left[(M_j^0)^2 + (M_k^0)^2 + (A^0_{ijk})^2\right]\right\} \\ & + \sum_{jk}\gamma_i^{jk}\left[(M_j^0)^2 + (M_k^0)^2 + (A^0_{ijk})^2\right]\ln(\mu^2_{\rm PV}/\mu_R^2) \\ & + \sum_a \gamma_i^a\left[3(M_a^0)^2 - (M_i^0)^2\right]\ln(\mu^2_{\rm PV}/\mu_R^2)\,, \end{aligned} \tag{43}$$

with M_i^0 being the tree-level scalar masses of (24).

To put these expressions into a less cumbersome form, we will consider the case where the various regularization weights p_{ia} and p_{jk} can be treated as one overall parameter p. The adoption of one overall regularization weight p makes it possible to identify the quantity

$$\ln(\mu^2_{\rm PV}/\mu_R^2) - p\ln\left[(t+\bar{t})|\eta(t)|^4\right] \equiv \ln(\widetilde{\mu}^2_{\rm PV}/\mu_R^2)$$

as a stringy threshold correction to the overall PV mass scale, or effective cut-off, $\mu_{\rm PV}$. Then inserting the tree-level

[2] Note that as we are considering the case with universal modular weights $n_i = -1$, these expressions can be reduced to $p_{ij} = 2 + \frac{1}{2}(q_i + q_j)$ and $p_{ia} = 2 + \frac{1}{2}(q_a + \hat{q}_i)$.

soft terms (24) into (39) and (43) yields these soft terms in the final form that we will use in the following analysis:

$$\begin{aligned} A_{ijk} &= -\frac{k_s}{3}F^S - \frac{1}{3}\gamma_i\overline{M} - p\gamma_i G_2\left(t,\bar{t}\right)F^T \\ &\quad + \tilde{\gamma}_i F^S \ln(\widetilde{\mu}^2_{\rm PV}/\mu^2_R) + \text{cyclic}(ijk) \qquad (44) \\ M_i^2 &= \left\{\frac{|M|^2}{9} - \frac{|F^T|^2}{(t+\bar{t})^2}\right\} \\ &\quad \times \left[1 + p\gamma_i - \left(\sum_a \gamma_i^a - 2\sum_{jk}\gamma_i^{jk}\right)\ln(\widetilde{\mu}^2_{\rm PV}/\mu^2_R)\right] \\ &\quad + (1-p)\gamma_i\frac{|M|^2}{9} + \left\{\widetilde{\gamma}_i\frac{MF^S}{6} + \text{ h.c. }\right\} \\ &\quad + \left\{p\widetilde{\gamma}_i G_2\left(t,\bar{t}\right)\frac{\overline{F}^T F^S}{2} + \text{ h.c. }\right\} + |F^S|^2 \\ &\quad \times \left[\left(\frac{3}{4}\sum_a \gamma_i^a g_a^4 + k_s k_{\bar{s}}\sum_{jk}\gamma_i^{jk}\right)\ln(\widetilde{\mu}^2_{\rm PV}/\mu^2_R)\right], \qquad (45) \end{aligned}$$

where $\widetilde{\gamma}_i$ is a shorthand notation for

$$\widetilde{\gamma}_i = \sum_a \gamma_i^a g_a^2 - k_s\sum_{jk}\gamma_i^{jk}\,. \qquad (46)$$

The one loop expressions of (30), (44) and (45) will be our starting point in the following two sections where we investigate their phenomenological significance in scenarios where tree-level soft supersymmetry breaking is suppressed or vanishing.

3 Classification of heterotic orbifold models

As a result of the assumptions made in Sect. 2, our general parameter space is defined by seven quantities, if we assume a tree-level Kähler potential for the dilaton of the form $k(S,\overline{S}) = -\ln(S+\overline{S})$ with $\langle s+\bar{s}\rangle = 2/g^2_{\rm STR} \simeq 4$. Three of these parameters represent scales: the gravitino mass $M_{3/2}$, the boundary condition scale $\mu_{\rm UV}$ at which the soft supersymmetry breaking terms appear and the Pauli–Villars cutoff scale $\mu_{\rm PV}$. The other four are parameters describing the moduli sector: the vacuum expectation value of the real part of the (uniform) Kähler modulus $\langle t+\bar{t}\rangle$, the modular weights of the PV regulators parameterized by p, the value of the Green–Schwarz coefficient $\delta_{\rm GS}$ and the Goldstino angle θ that determines the degree to which the dilaton and moduli F-terms participate in the transmission of supersymmetry breaking.

3.1 Moduli dominated scenarios

This section assumes that i) all fields have modular weight $n_i = -1$, which gives a no-scale structure, and ii) we have moduli-dominated supersymmetry breaking (θ vanishes, $\cos\theta = 1$), so that the tree-level soft terms are precisely zero. In addition, those loop-induced soft terms in (45) proportional to tree level quantities are also zero, leaving only those arising from the superconformal anomaly and those related to the Pauli–Villars sector:

$$\begin{aligned} M_a &= \frac{g_a^2(\mu)}{2}\left\{2\left[\frac{\delta_{\rm GS}}{16\pi^2} + b_a\right]G_2\left(t,\bar{t}\right)F^T + \frac{2}{3}b_a\overline{M}\right\}, \\ A_{ijk} &= -\frac{1}{3}\gamma_i\overline{M} - p\gamma_i G_2\left(t,\bar{t}\right)F^T + \text{cyclic}(ijk)\,, \\ M_i^2 &= (1-p)\gamma_i\frac{|M|^2}{9}\,. \qquad (47) \end{aligned}$$

Note that in the special case where the moduli are stabilized at one of their two self-dual points $t=1$ and $t=e^{{\rm i}\pi/6}$, we recover the universal "anomaly mediated" results

$$\begin{aligned} M_a &= g_a^2(\mu)\, b_a\frac{\overline{M}}{3} \\ A_{ijk} &= -\left(\gamma_i+\gamma_j+\gamma_k\right)\frac{\overline{M}}{3} \\ M_i^2 &= (1-p)\gamma_i\frac{|M|^2}{9}\,. \qquad (48) \end{aligned}$$

The scenario that has come to be referred to as the "anomaly mediated supersymmetry breaking" (AMSB) scenario [1–3], in which scalar masses first appear only at two loops, is obtained in the limit as the phenomenological parameter p approaches unity. This would be the case, for example, if the mass-generating Pauli–Villars fields Π^A had the same Kähler metric as the regulator fields Φ^A and thus $q_i = -1$, $\hat{q}_i = 1$ and $q_a = -3$. In any event, it is clear that the parameter p defines a family of "anomaly mediated" models for the case of moduli stabilized at self-dual points. Importantly, for $p < 1$, as would be typical in orbifold models, the anomaly-mediated masses for the matter scalars are positive with only the Higgs fields having negative squared masses at the scale $\mu_{\rm UV}$.

The contrast between these results and those of the standard AMSB case was discussed in [5,6], but it is important to point out that the vanishing of the scalar masses at one loop in the $p \to 1$ limit clearly demands a two-loop analysis of these soft terms. A treatment of supergravity radiative corrections, regularized by the Pauli–Villars mechanism, at two loops would be a massive undertaking. Some subset of these corrections would undoubtedly be the soft terms found in [2,3] using a spurion technique. As is now well-known, these two-loop terms arising from the superconformal anomaly would imply negative squared masses for the scalar leptons. To remedy this situation, the AMSB model, as it has been institutionalized in studies such as the Snowmass Points and Slopes [22], adopts an otherwise ad hoc scalar mass contribution that is universal and sufficiently large. Not surprisingly, these models are often characterized as having light sleptons as a key feature of the phenomenology.

While several extensions of the original (or "minimal") AMSB model now exist that address the slepton mass problem in a variety of ways,[3] the generalized anomaly me-

[3] For some early solutions, see [23].

diated model we present here suffers from no such problem when $p \neq 1$. While the phenomenology associated with the gaugino mass spectrum is familiar from past studies of the AMSB paradigm, the scalar mass sector looks quite different. We will begin our analysis in Sect. 5.2 with this generalized anomaly mediated model (which we will refer to as the "PV–AMSB model") before enlarging the parameter space to include all moduli-dominated models in Sects. 5.3 and 5.4.

3.2 Dilaton dominated scenarios with Kähler suppression

We next turn to the opposite extreme, where the dilaton is the primary source of supersymmetry breaking in the observable sector ($\sin\theta = 1$). In such a scenario we would ordinarily expect the loop corrections such as those in (25), (39) and (43) to be small perturbations on the dominant (and universal) tree-level contributions and thus safely neglected. The phenomenology of the dilaton domination scenario at tree-level has been extensively studied in the literature [24].

The bulk of these studies, however, have considered only the case of the standard Kähler potential $k(S,\overline{S}) = -\ln(S+\overline{S})$ derived from the tree-level string theory. It is well-known that when this form is used, stabilizing the dilaton at acceptable weak-coupling values is extremely difficult. In the case where a dilaton potential is imagined to arise through field theory nonperturbative effects (such as gaugino condensation) it has been shown that one condensate alone can never succeed in stabilizing the dilaton in such a way as to reproduce the weak coupling observed in nature [25, 26]. Furthermore, while multiple condensates can be used to provide the requisite stabilization [27, 28], these models tend to predict a moduli-dominated scenario such as those in Sect. 3.1.

In contrast, if one postulates a nonperturbative correction of stringy origin to the dilaton Kähler potential, as was first motivated by Shenker [29], then one condensate can indeed stabilize the dilaton at weak coupling while simultaneously ensuring vanishing vacuum energy at the minimum of the potential. The power of this approach was first demonstrated in an explicit model of modular invariant gaugino condensation in [7, 8] and confirmed in [30], providing a concrete realization of the so-called "generalized dilaton domination scenario" [26].

The key feature of such models is the deviation of the dilaton Kähler metric from its tree-level value. If we imagine the superpotential for the dilaton having the form $W(S) \propto e^{-3S/2b_+}$, with b_+ being the largest beta-function coefficient (26) among the condensing gauge groups of the hidden sector, then it is clear from (7) and (8) that requiring the potential (6) to vanish implies

$$(k^{s\bar{s}}) \left| k_s - \frac{3}{2b_+} \right|^2 = 3 \rightarrow (k^{s\bar{s}})^{-1/2} = \sqrt{3}\frac{\frac{2}{3}b_+}{1-\frac{2}{3}b_+k_s} \,. \tag{49}$$

The condition in (49) is independent of the means by which the dilaton is stabilized and is a result merely of requiring a vanishing vacuum energy in the limit of dilaton-domination. The explicit model of [8], however, was able to achieve precisely this relation with $\langle k_s \rangle = -g_{\rm STR}^2/2$, using a correction to the dilaton action that involved tuning $\mathcal{O}(1)$ numbers only.[4]

We can parameterize the departure that (49) represents from the tree-level Kähler metric $\left\langle (k_{s\bar{s}}^{\rm tree})^{1/2} \right\rangle = \langle 1/(s+\bar{s}) \rangle = g_{\rm STR}^2/2 \simeq 1/4$ by introducing the phenomenological parameter

$$a_{\rm np} \equiv \left(\frac{k_{s\bar{s}}^{\rm tree}}{k_{s\bar{s}}^{\rm true}} \right)^{1/2} , \tag{50}$$

so that the auxiliary field of the dilaton chiral supermultiplet can be expressed as

$$F^S = \sqrt{3} M_{3/2} (k_{s\bar{s}})^{-1/2} = \sqrt{3} M_{3/2} a_{\rm np} (k_{s\bar{s}}^{\rm tree})^{-1/2} \,. \tag{51}$$

The importance of (49) for our purposes is to recognize that the factor of b_+, containing as it does a loop factor, will suppress the magnitude of the auxiliary field F^S relative to that of the supergravity auxiliary field M through the relation (51). Therefore, tree-level soft terms for the gaugino masses and trilinear A-terms will be of comparable magnitude to the loop-induced soft terms arising from the superconformal anomaly (though scalar masses will be only negligibly altered from their tree level values). We are thus led to consider the phenomenology of models given by the following pattern of soft supersymmetry breaking terms:

$$\begin{aligned}
M_a &= \frac{g_a^2(\mu)}{2} \left\{ \frac{2}{3} b_a \overline{M} + [1 - 2b_a' k_s] F^S \right\} \\
A_{ijk} &= -\frac{k_s}{3} F^S - \frac{1}{3} \gamma_i \overline{M} + \tilde{\gamma}_i F^S \ln(\tilde{\mu}_{\rm PV}^2/\mu_R^2) + \text{cyclic}(ijk) \\
M_i^2 &= \frac{|M|^2}{9} \left[1 + \gamma_i - \left(\sum_a \gamma_i^a - 2 \sum_{jk} \gamma_i^{jk} \right) \ln(\tilde{\mu}_{\rm PV}^2/\mu_R^2) \right] \\
&\quad + \left\{ \tilde{\gamma}_i \frac{M F^S}{6} + \text{ h.c. } \right\} ,
\end{aligned} \tag{52}$$

where we have dropped terms of $\mathcal{O}\left(1/(16\pi^2)^3\right)$ in the scalar masses. These models will be studied in Sect. 5.5.

4 Experimental and cosmological constraints

In order to translate the spectra defined by the soft supersymmetry breaking terms in Sects. 3.1 and 3.2, a low en-

[4] In fact, the model considered in this reference used the linear multiplet formalism for the dilaton in which such nonperturbative corrections are more easily incorporated into the low energy effective supergravity theory. For a description on how to correctly translate from one formulation to the other, see Appendix A of [6].

ergy soft Lagrangian is obtained by solving the renormalization group equations (RGEs) from some initial boundary condition scale to the electroweak scale. Having thus extracted the soft supersymmetry breaking parameters at the low-energy scale, the physical mass spectra for the superpartner and Higgs sector can be obtained and various direct collider constraints and indirect non-collider constraints can be applied to examine the region of phenomenological viability of these models. In this section, we describe the tools that we use and the various observational constraints that we impose.

4.1 Electroweak symmetry breaking and physical masses

We have used the Fortran code SuSpect [31] to solve the RGEs for the soft supersymmetry breaking parameters between the initial high energy scale $\mu_{\rm UV}$ and the scale given by the Z-boson mass. While the initial scale $\mu_{\rm UV}$ should itself be treated as a model-dependent parameter, we have chosen $\mu_{\rm UV} = \mu_{\rm GUT}$ throughout. We use $\tan\beta$ and the sign of the supersymmetric μ parameter in the superpotential as free parameters, defined at the low-energy (electroweak) scale.

The magnitude of the μ parameter is determined by imposing electroweak symmetry breaking (EWSB) at the scale defined by the geometric mean of the two stop masses $(m_{\tilde{t}_1} m_{\tilde{t}_2})^{1/2}$, which minimizes the one-loop scalar effective potential [32, 33]. The one-loop corrected μ term is obtained from the condition

$$\bar{\mu}^2 = \frac{\left(m_{H_d}^2 + \delta m_{H_d}^2\right) - \left(m_{H_u}^2 + \delta m_{H_u}^2\right)\tan\beta}{\tan^2\beta - 1} - \frac{1}{2}M_Z^2\,, \tag{53}$$

where $\delta m_{H_u}^2$ and $\delta m_{H_d}^2$ represent the one loop tadpole corrections to the running Higgs masses $m_{H_u}^2$ and $m_{H_d}^2$ [34–36]. SuSpect includes the corrections from all the third generation fermion and sfermion loops as well as loops from gauge bosons, Higgs bosons, charginos and neutralinos. As the superpartner spectrum depends on the value of the μ parameter computed in (53), the proper inclusion of superpartner thresholds in the RG evolution requires that the procedure be iterated until a coherent and stable value for μ is obtained. Usually, SuSpect requires only two or three iterations to have a relative precision of the order of 10^{-4}. We have used three. The soft supersymmetry breaking parameters at the weak scale are then passed to the C code micrOMEGAs [37] to perform the calculation of physical masses for the superpartners and various indirect constraints, to be described in the following section.

The specific algorithm that we employ can be described as follows. The one-loop order SUSY breaking parameters of the heterotic orbifold models obtained in the previous section are entered into SuSpect at the high energy scale. Other parameters, including standard model fermion masses and gauge weak couplings, as well as certain EWSB parameters such as $\tan\beta$ are input at the low energy scale. SuSpect runs the renormalization group evolution of the parameters back and forth between the low energy scales such as M_Z and the electroweak symmetry breaking scale, and the high-energy scale such as the GUT scale. This is the case for the soft SUSY-breaking terms (scalar and gaugino masses, bilinear and trilinear couplings and $\tan\beta$) and μ. This procedure has to be iterated in order to include SUSY threshold effects or radiative corrections due to Higgs and SUSY particles. In the first step, these thresholds are only guessed, since the spectrum has not been calculated yet, and the radiative corrections are not implemented. The thresholds are properly taken into account in subsequent iterations. At the electroweak scale, the consistency in the calculation of the μ term is checked using the expression in (53). We then call micrOMEGAs, which calculates the SUSY spectrum at one-loop order using FeynHiggs for the Higgs sector. micrOMEGAs also calculates the $b \to s\gamma$ branching ratio, as well as the relic density of the lightest neutralino and the anomalous magnetic moment of the muon. We have checked the consistency between the two spectra generated by SuSpect and by micrOMEGAs: the maximum deviation was of the order of 4% and was confined to specific regimes such as high $\tan\beta$.

The first condition that we require on a given set of soft supersymmetry breaking masses is that an appropriate vacuum state appears — in particular that EWSB occurs. Clearly it is possible for the value of $\overline{\mu}^2$ in (53) to become negative for a particular choice of model parameters. In such a situation EWSB does not occur. The precise domain of parameter space where this occurs is sensitive to the values of the Yukawa couplings — and hence to the choice of quark pole masses assumed. This makes the SUSY corrections to the bottom quark mass quite important. We have performed the analysis using the heavy fermion masses in SuSpect of

$$M_t = 175.0\,\text{GeV}, \quad M_b = 4.62\,\text{GeV}, \quad M_\tau = 1.778\,\text{GeV}\,, \tag{54}$$

and gauge couplings at the Z-mass of

$$\alpha_{\rm EM}^{\overline{MS}}(M_Z) = 1/127.938, \quad \alpha_s^{\overline{MS}}(M_Z) = 0.118,$$
$$\bar{s}_W^2 = 0.23117\,. \tag{55}$$

We also reject all points in the parameter space that give a tachyonic Higgs boson mass (in particular, where $m_A^2 < 0$) or negative sfermion squared masses.

We next require that the lightest supersymmetric particle (LSP) be neutral, and thus also reject all model parameters where the lightest neutralino $\widetilde{\chi}_1^0$ is not the LSP. In most of the rejected cases it is the lightest stau $\widetilde{\tau}_1$ or the gluino $\tilde{g}$ that becomes lighter than $\widetilde{\chi}_1^0$. The remaining parameter space is further reduced by limits on the superpartner and Higgs masses from various collider experiments.

Concerning the mass bounds that we use, we take the most recent results combined by the LEP Working Group [38, **?**]. For the light CP-even neutral Higgs mass ($m_{\rm h}$), we assume that a 95% confidence level (CL) lower limit on $m_{\rm h}$ is set at 111.5 GeV. The search for an invisibly decaying Higgs boson in hZ production has allowed

a 95% CL lower limit on $m_{\rm h}$ to be set at 114.4 GeV, assuming a production cross section equal to that in the standard model and a 100% branching fraction to invisible decays [39]. We believe the value of 113.5 GeV serves as a good reference point, and this is the value we use in our analysis. Concerning the chargino limit, we take 103.5 GeV, bearing in mind that in some degenerate cases and for light sleptons, the limit can go down to 88 GeV [40]. For the squark sector, the limit of 97 GeV [41] is implemented. For all mass bounds we should keep in mind that experimental limits are always given in the context of a particular SUSY model, which is not generally a string motivated one. The bounds that we use could possibly be weakened in some cases.

4.2 Indirect constraints on supersymmetric spectra

Various non-collider observations can be used to reduce the allowed parameter space of these loop-dominated orbifold models. We will focus our attention on the three such processes that yield the most stringent constraints: the density of relic neutralino LSPs, the branching ratio for decays involving the process $b \to s\gamma$ and the measurement of the anomalous magnetic moment of the muon.

4.2.1 The relic neutralino density

The existence of dark matter is one of the first glimpses of possible physics beyond the standard model. It is probable that dark matter consists of some stable or extremely long-lived particle left over from the hot early universe. For any given extension of the standard model containing stable or long-lived particles, the present-day relic density of such particles can prove quite constraining. The basic calculation of a relic density from thermal considerations is standard [42]. Here we review the steps in such a calculation under the explicit assumption that the lightest neutralino constitutes the cold dark matter particle.

The initial number density of the neutralino is determined because the particle is assumed to have been in thermal equilibrium. When the particle begins in thermal equilibrium with its surroundings, interactions that create neutralinos usually happen as frequently as reverse interactions that destroy neutralinos. Once the temperature drops below $T \simeq m_\chi$, most particles no longer have sufficient energy to create neutralinos. Now neutralinos can only annihilate, and these annihilations occur until about the time when the Hubble expansion parameter becomes larger than the annihilation rate, $H \geq \Gamma_{\rm ann}$. When expansion dwarfs annihilation, neutralinos are separated from each other too quickly to maintain equilibrium. This happens at the freeze-out temperature, usually at $T_{\rm F} \simeq m_\chi/20$ for cold dark matter.

In most neutralino relic density calculations, the only interaction cross sections that need to be calculated are annihilations of the type $\chi\chi \to X$, where χ is the lightest neutralino and X is any final state involving only standard model particles. However, there are scenarios in which other particles in the thermal bath have important effects on the evolution of the neutralino relic density. Such a particle annihilates with the neutralino into standard model particles and is called a coannihilator [43]. To serve as an effective coannihilator, the particle must have direct interactions with the neutralino and must be nearly degenerate in mass. Such degeneracy happens in MSSM, for instance, with possible coannihilators being the lightest stau [44], the lightest stop [45], the second-to-lightest neutralino or the lightest chargino [46, 47]. When this degeneracy occurs, the neutralino and all relevant coannihilators form a coupled system. In this section, we will denote particles belonging to that coupled system by χ_i. Now all interactions involving particles in this coupled system come into play, including $\chi_i\chi_j \to X$, $\chi_i X \to \chi_j Y$, and $\chi_i \to \chi_j X$. Here both X and Y denote states including standard model particles. Decays once again enter the calculation because the coannihilators are generally not stable and eventually decay into the lightest neutralino.

For the case without coannihilations, evolution of the relic particle number density, n, happens in accordance with the single species Boltzmann equation

$$\frac{{\rm d}n}{{\rm d}t} = -3Hn - \langle\sigma v\rangle \left[n^2 - (n^{\rm eq})^2\right] , \qquad (56)$$

where $n^{\rm eq}$ is the equilibrium number density, H is the Hubble parameter at time t, and $\langle\sigma v\rangle$ is the thermally averaged annihilation cross section. The number density is modified by Hubble expansion and by direct and inverse annihilations of the relic particle. The relic particle is assumed to be stable, so relic decay is neglected. In the above expression, we have also assumed T invariance to relate annihilation and inverse annihilation processes.

In the presence of coannihilators, the Boltzmann equation becomes more complicated but can be simplified using the stability properties of the relic particle and the coannihilators (using $n = \sum_{i=1}^{N} n_i$). Application of these simplifications leads to

$$\frac{{\rm d}n}{{\rm d}t} = -3Hn - \sum_{i,j=1}^{N} \langle\sigma_{ij} v_{ij}\rangle \left(n_i n_j - n_i^{\rm eq} n_j^{\rm eq}\right) . \qquad (57)$$

To a very good approximation, one can use the usual single species Boltzmann equation for the case of coannihilations if the following replacement is made for the thermally averaged cross section:

$$\langle\sigma v\rangle = \sum_{i,j} \langle\sigma_{ij} v_{ij}\rangle \frac{n_i^{\rm eq}}{n^{\rm eq}} \frac{n_j^{\rm eq}}{n^{\rm eq}} . \qquad (58)$$

For scenarios involving coannihilations, the expression for the thermally averaged cross section begins as a six-dimensional integral, seven-dimensional including the integration over the final state angle. This integral has been conveniently put into the form of a one-dimensional integral over the total squared center of mass energy [48]. Computer codes exist that numerically perform the center of mass momentum integration and the final state angular integration. Some codes include only a subset of all possible coannihilation channels [49, 50], while the program

micrOMEGAs includes all relevant coannihilation channels. Analytical expressions for the cross sections after integration over the final state angle also exist in the literature [51]. In practice, the Boltzmann equation is generally not given a full numerical treatment since accurate approximate solutions exist [42].

Once the effective thermally averaged cross section has been derived as a function of temperature, it is used to iteratively determine the freeze-out temperature. In practice, the dimensionless inverse freeze-out temperature, $x_{\rm F} = m_\chi/T_{\rm F}$, is calculated using

$$x_{\rm F} = \ln\left(\frac{0.038 g m_{\rm PL} m_\chi \langle\sigma v\rangle}{\sqrt{g_* x_{\rm F}}}\right) . \tag{59}$$

Here $m_{\rm PL}$ is the Planck mass, g is the total number of degrees of freedom of the χ particle (spin, color, etc.), g_* is the total number of effective relativistic degrees of freedom at freeze-out, and the thermally averaged cross section is evaluated at the freeze-out temperature. For most cold dark matter candidates, $x_{\rm F} \simeq 20$.

When the freeze-out temperature has been determined, the total (co)annihilation depletion of the neutralino number density can be calculated by integrating the thermally averaged cross section from freeze-out to the present temperature (essentially $T = 0$). The thermally averaged cross section appears in the formula for the relic density in the form of the integral $J(x_{\rm F}) = \int_{x_{\rm F}}^{\infty} \langle\sigma v\rangle x^{-2}\,{\rm d}x$:

$$\Omega_\chi h^2 = 40\sqrt{\frac{\pi}{5}}\frac{h^2}{H_0^2}\frac{s_0}{m_{Pl}^3}\frac{1}{\left(g_{*S}/g_*^{1/2}\right) J(x_{\rm F})} . \tag{60}$$

Here g_{*S} is the number of effective relativistic degrees of freedom contributing to the entropy of the universe and h is the reduced Hubble parameter, defined by $H_0 = 100\,{\rm h\,km\,s^{-1}Mpc^{-1}}$. The above expression is commonly given in the less explicit form:

$$\Omega_\chi h^2 = \frac{1.07\times 10^9\,{\rm GeV}^{-1}}{g_*^{1/2} m_{\rm PL} J(x_{\rm F})} . \tag{61}$$

This is the expression that one compares with an experimental determination of the dark matter abundance.

Recent evidence suggests [52] that $\Omega_\chi \sim 0.3$ with $h^2 \sim 0.5$. We will take as a conservative favored region,

$$0.1 < \Omega_\chi h^2 < 0.3 . \tag{62}$$

The lower bound comes from the requirement that χ_1^0 should at least form galactic dark matter, and the upper bound is a very conservative interpretation of the lower bound on the age of the Universe. Recently, WMAP [53] has elegantly confirmed the composition of the Universe to be 73% dark energy and 27% matter. WMAP determines a total matter density $\Omega_{\rm M} h^2 = 0.135^{+0.008}_{-0.009}$ and a total baryon density $\Omega_{\rm B} h^2 = 0.0224 \pm 0.0009$, from which one can extract a 2σ range for the density of cold dark matter: $\Omega_{\rm CDM} h^2 = 0.1126^{+0.0161}_{-0.0181}$. The effect of the WMAP measurement has been studied in the case of neutralino dark matter from mSUGRA [54] and rSUGRA [55] and also in the case of scalar dark matter from 'little Higgs' theories [56]. We use the more conservative numbers in (62) in the figures to follow. However, we comment on the changes if the WMAP results are applied. Let us stress that the requirement of (62) should not be treated as a constraint, but rather as an indication of the region preferred by cosmological considerations. Theoretical assumptions made to extract the present relic density of neutralino LSPs need not hold. In fact, the missing non-baryonic matter in the universe may not consist of relic neutralinos at all.

4.2.2 The $b \to s\gamma$ constraint

Another observable where the supersymmetric contribution can be important and measurable is the flavor changing decay $b \to s\gamma$ [57]. In the standard model, this process is mediated by virtual isospin $+1/2$ quarks and W-bosons. In supersymmetric theories, the spectrum allows new contributions involving loops of charginos and squarks or top quarks and charged Higgs bosons. As these two contributions appear at the same order of perturbation theory, the measurement of the inclusive decay $B \to X_s\gamma$ is a powerful tool in the search for physics beyond the standard model. For our analysis, we will use the results given by the CLEO and BELLE collaborations [58].

The particle data group [59] summarizes these results and gives the current limit as:

$$BR(b \to s\gamma) = (3.37 \pm 0.37 \pm 0.34 \pm 0.24^{+0.35}_{-0.16} \pm 0.38)\,10^{-4} , \tag{63}$$

where the three first errors represent, respectively, the statistical errors, the systematic error, and the estimated error on the model describing the behavior of the quarks in the B-meson decay. The fourth uncertainty is the error made by an extrapolation to the entire energy range for the photon (cut at 2.1 GeV for the experiment). The last error value is an estimate of the theoretical uncertainties. To be as conservative as possible, one could add linearly all the uncertainties of (63). However, we will adopt the procedure taken in the recent benchmark study of Battaglia et al. [60] and choose to impose the constraint

$$2.33\times 10^{-4} < BR(b \to s\gamma) < 4.15\times 10^{-4} . \tag{64}$$

Let us note that we perform these calculations under the assumptions of minimal flavor violation.

4.2.3 The muon anomalous magnetic moment

The relation between the spin s of the muon and its magnetic moment μ is given classically by $\mu = g_\mu \frac{e\hbar}{2m_\mu c} s$, where $g_\mu = 2(1 + a_\mu)$. Following [61], we introduce the parameter δ_μ to quantify the difference between theoretical and experimental determinations of a_μ:

$$\delta_\mu \equiv (a_\mu - 11\,659\,000\times 10^{-10})\times 10^{10} . \tag{65}$$

The Brookhaven collaboration has reported a measurement of the anomalous magnetic moment of the muon [62]

$$\frac{(g_\mu^{\rm exp}-2)}{2} = a_\mu^{\rm exp} = (11\,659\,202 \pm 14 \pm 6) \times 10^{-10}\,, \tag{66}$$

where the first error is statistical uncertainty and the second is systematic uncertainty. From this, the current experimental determination of the parameter δ_μ is $\delta_\mu^{\rm exp} = 203 \pm 8$.

To understand the implications of this result for supersymmetry, one needs to know the standard model contribution. Unfortunately, the computation of $\delta_\mu^{\rm SM}$ in the standard model is complicated by our poor understanding of the hadronic contributions to certain vacuum polarization diagrams. The theoretical result depends on whether one uses the e^+e^- annihilation cross section or τ decay data to estimate these contributions, and continues to change over time as the calculation is refined [63]:

$$\delta_\mu^{\rm exp} - \delta_\mu^{\rm SM} = (22.1 \pm 7.2)10^{-10} \quad [e^+e^-] \tag{67}$$

$$\delta_\mu^{\rm exp} - \delta_\mu^{\rm SM} = (7.4 \pm 5.8)10^{-10} \quad [\tau\text{-decay}]\,, \tag{68}$$

corresponding to a discrepancy between the standard model prediction and experiment of, respectively, 1.9 and 0.7 standard deviations. In our discussion, we will be less conservative than the authors of [61] and consider a roughly three standard deviation region about the anomalous moment of the muon based on the τ decay analysis:

$$-11.6 < \delta_\mu^{\text{new physics}} = \delta_\mu^{\rm exp} - \delta_\mu^{\rm SM} < 30.4 \quad [3\,\sigma]\,. \tag{69}$$

The contribution of SUSY particles to the anomalous moment of the muon mainly comes from neutralino-smuon and chargino-sneutrino loop-induced processes. As the chargino/slepton/lepton couplings have the same form as the chargino/squark/quark couplings, the parameter space restriction imposed by the constraint (69) will be similar in many respects to the one given by the $b \to s\gamma$ process. Thus, the SUSY contribution to $(g_\mu - 2)$ is large for large values of $\tan\beta$ and small values of the soft-breaking masses. It is interesting to note that the sign of the SUSY contribution is equal to the sign of the μ parameter. With our conventions this implies that positive μ is favored, as in the $b \to s\gamma$ constraint [57].

Let us briefly summarize the above-mentioned constraints that are to be applied below. First, we demand that electroweak symmetry be correctly broken, as defined by deriving a positive value for $\bar{\mu}^2$ from (53). It should be noted that we use parameters of the standard model as defined in (54) and (55). Next, we demand that the mass of the lightest scalar Higgs boson be greater than or equal to 113.5 GeV. Additionally, we require that the mass of the lightest chargino be greater than or equal to 103.5 GeV. We also require that the lightest slepton mass be larger than 88 GeV and the lightest squark mass be greater than 97 GeV, but these two scalar fermion mass limits exclude no regions of parameter space in the plots resulting from our analysis. We also indicate regions of parameter space that result in the right thermal abundance of relic neutralinos: $0.1 \leq \Omega_\chi h^2 \leq 0.3$. While we technically do not exclude any regions solely for failing to produce the cosmologically preferred relic density, we do require that the lightest neutralino be the LSP. In terms of the flavor changing decay $b \to s\gamma$, we take a conservative approach and require the branching ratio to obey $2.33 \times 10^{-4} < BR(b \to s\gamma) < 4.15 \times 10^{-4}$, given in (64). Finally, we follow the recent τ decay analysis of the muon anomalous magnetic moment and require $-11.6 < \delta_\mu^{\text{new physics}} < 30.4$, given above in (69).

5 Results and analysis

We are now in a position to investigate the way in which low energy observations can distinguish different regions of the weakly-coupled heterotic string parameter space. We first recall the standard analysis in the context of the minimal supergravity (mSUGRA) parameter space. While the unified mSUGRA paradigm is unlikely to find a manifestation in realistic string-based models, it nonetheless provides a useful benchmark for calibrating results from one study to the next.

5.1 Revisiting mSUGRA

The minimal supergravity paradigm is based on the assumption that the soft supersymmetry breaking Lagrangian is determined by only five parameters. These include a universal gaugino mass $M_{1/2}$, a universal scalar mass M_0 and a universal trilinear soft parameter A_0, as well as the sign of the μ parameter and $\tan\beta$. A quick survey of the soft terms presented in Sect. 3 indicates that there is no point in the parameter space of the string models that we consider that generates such a universal outcome. A unified scenario is possible only in the event that the tree-level dilaton domination case arises [24], though no explicit realization of this outcome exists in a complete model. Even if such a scenario were realized, the soft terms would be constrained to a particular point of the mSUGRA parameter space such that

$$-A_0 = M_{1/2} = \sqrt{3} M_0\,. \tag{70}$$

Despite this lack of theoretical motivation, the extreme simplicity of the mSUGRA approach makes it an attractive scenario for phenomenological study [64]. We will here just present the main outcomes of our analysis. There are still large areas of parameter space in the $(M_{1/2}, M_0)$ plane that are allowed, particularly for large $\tan\beta$ where the Higgs mass bound is less constraining. The constraint from the process $b \to s\gamma$ can be the dominant constraint for low gaugino masses. Nevertheless, it is never very severe for positive μ, even for high $\tan\beta$ (note the change in scale in Fig. 2 relative to Fig. 1). The situation would change in the case of large trilinear A-terms because of the possibility of light

third generation squarks [45]. However, in this case, charge and/or color breaking (CCB) problems often arise.

In both plots of Fig. 1 the exclusion regions for the chargino and Higgs masses are given. These exclusion regions implement the experimental limits of 103.5 and 113.5 GeV, respectively, that were discussed in Sect. 4.1. We also provide contours of constant Higgs mass of $m_{\rm h} = 115.5$ GeV and 117 GeV (the dashed lines from left to right) as well as a contour of chargino mass $m_{\chi_1^\pm} = 500$ GeV (dotted line). For small and moderate values of $\tan\beta$, the requirement that the density of the lightest neutralino accounts for the dark matter density is very constraining and sensitive to the precise value of $\tan\beta$. For moderate and low values of this parameter, one usually finds too much relic density in the mSUGRA model. For example, the "bulk" region at low scalar and gaugino masses is excluded by the Higgs mass limit. Only three regions survive: a narrow band along the $\widetilde{\tau}$-LSP exclusion zone, a large Higgs pole region at extremely high $\tan\beta$, and the "focus point" [65] region at high values of M_0 (the thin strip along the "no EWSB" region in Fig. 2). The region next to the $\widetilde{\tau}$-LSP exclusion zone provides for efficient $\widetilde{\tau}_1\widetilde{\chi}_1^0$ coannihilation, considerably reducing the neutralino density. For high values of $\tan\beta$, interesting areas exist where $\Omega_\chi h^2$ becomes smaller due to near-resonant s-channel annihilation through the heavy Higgs states (A or H). Here m_A and m_H become smaller and their couplings to the b quark and the τ lepton increase. In this region $\widetilde{\chi}_1^0\widetilde{\chi}_1^0 \to b\overline{b}, \tau^+\tau^-$ dominates and causes significant depletion of the relic density. This can clearly be seen in the plot for $\tan\beta = 50$. It should be noted that these results are strongly dependent on the treatment of the radiative correction for the bottom mass and the Higgs masses. As stated earlier, we have taken $M_{\rm b} = 4.62$ GeV. Small changes in these values have dramatic consequences on the density. At large M_0 and small $M_{1/2}$ there is another region (the "focus point" region) where the lightest neutralino as well as the lightest chargino acquire relatively small mass and large Higgsino components. The coupling to the bosons W and Z is large enough to make the annihilation process into WW or ZZ efficient. If the WMAP measurement is used instead, then the areas labeled "Ω" collapse to thin lines around the lower value of $\Omega_\chi h^2 = 0.1$. In both of the figures, this value prefers lower values of the mass parameters.

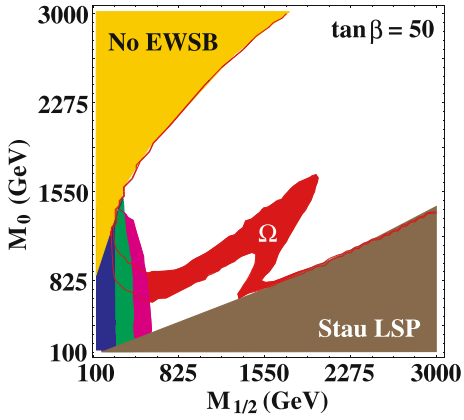

Fig. 2. Constraints on the mSUGRA parameter space for $\tan\beta = 50$. Constraints on the $(M_{1/2}, M_0)$ mSUGRA plane are given for $\mu > 0$ and $A_0 = 0$. Note the change in scale relative to Fig. 1. The *red region* represents the $0.1 < \Omega_\chi h^2 < 0.3$ preferred region. The three *shaded regions* in the *lower left* are excluded by (from left to right) the chargino mass limit, the lightest Higgs boson mass limit and the $b \to s\gamma$ rate

Our results are in agreement with the previous studies of mSUGRA [64]. The only discrepancies appear in the high $\tan\beta$ regimes, mostly due to the different treatment of the b-quark mass and associated Yukawa coupling, and the Higgs sector masses. These differences can be understood in the light of the work done by Allanach et al. [66]. Indeed,

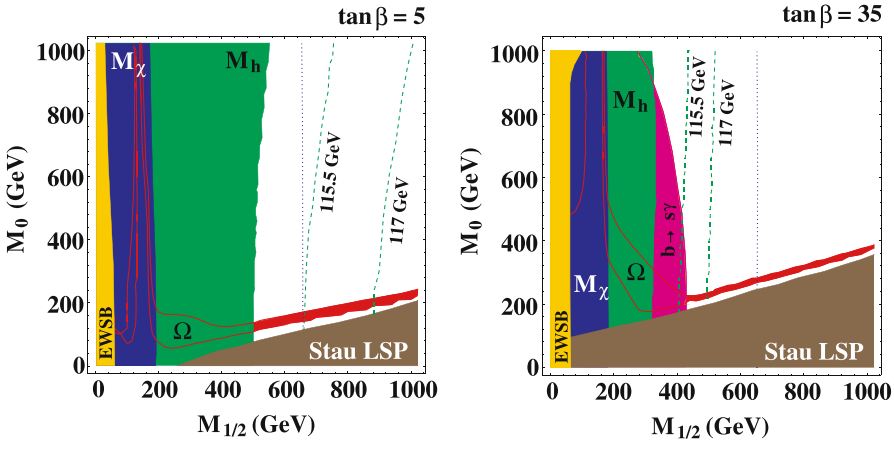

Fig. 1. Constraints on the mSUGRA parameter space for $\tan\beta = 5$ (*left*) and $\tan\beta = 35$ (*right*). Constraints on the $(M_{1/2}, M_0)$ mSUGRA plane are given for $\mu > 0$ and $A_0 = 0$. The *red contours* and *shaded region* represent the $0.1 < \Omega_\chi h^2 < 0.3$ preferred region. A small region at very low gaugino masses marked "EWSB" is ruled out by improper EWSB. Contours of constant Higgs mass of $m_{\rm h} = 115.5$ GeV and 117 GeV (the *dashed lines* from left to right) as well as a contour of chargino mass $m_{\chi_1^\pm} = 500$ GeV (*dotted line*) are given. For a description of the experimental constraints applied, see Sect. 4

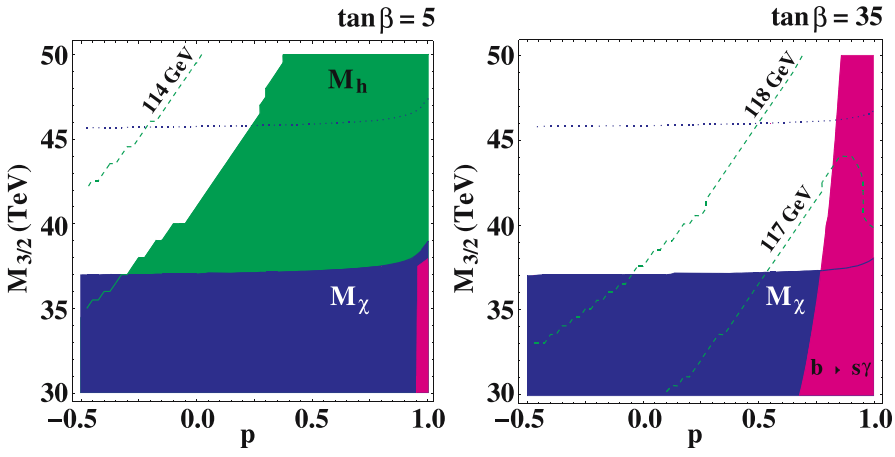

Fig. 3. Constraints on the PV-AMSB parameter space for $\tan\beta = 5$ (*left*) and $\tan\beta = 35$ (*right*). Constraints on the $(M_{3/2}, p)$ plane are given for $\mu > 0$. The regularization weight p can be as large as $p = 1$, at which point scalar masses vanish at the one loop level (the standard AMSB limit). The areas marked M_χ and M_h are ruled out by the chargino mass bound and the Higgs mass bound, respectively. The area marked $b \to s\gamma$ gives $Br(b \to s\gamma) \geq 4.15 \times 10^{-4}$ (a small region where this bound is relevant occurs near $p = 1$ for $\tan\beta = 5$). The *horizontal* (*dotted*) *contour* is a constant chargino mass of $m_{\chi_1^\pm} = 130\,\mathrm{GeV}$

the treatment of the Yukawa coupling of the $b-$quark (λ_b) in SuSpect results in a higher value for λ_b than from the other publicly available codes (a 4 to 8 percent effect). This discrepancy affects the Higgs masses (m_A in particular) via the RGEs, which are dominated by λ_b for high $\tan\beta$. For instance, for $\tan\beta = 50$, we can easily find a 20 to 50 GeV difference for m_A, explaining differences in the parameter space allowed by the relic density in the A-pole sector. In the remainder of our paper, we will restrict ourselves to $\tan\beta \leq 35$. In this range, the discrepancies between codes are smaller than 3 percent. In terms of relic densities, the differences between results using the codes DarkSusy [50] and micrOMEGAs [37] come from both the b-mass treatment and the selection of included coannihilation channels: previous versions of DarkSusy did not include any coannihilation channels with sleptons and scalars while micrOMEGAs does.[5]

To summarize, in the case of the mSUGRA model, even if large areas of the $(M_{1/2}, M_0)$ parameter space are still allowed by present accelerator data, combining the $b \to s\gamma$ limits, the neutralino relic density constraints and the Higgs mass limit selects the $\widetilde{\tau}$ coannihilation region, the "focus point" region, or extremely high values of $\tan\beta$. These three regions represent the extreme boundaries of mSUGRA. Thus, it is natural go beyond mSUGRA to see how these constraints affect orbifold models.

5.2 Moduli domination: the anomaly-mediated limit

The phenomenology of the original (minimal) AMSB model has been extensively studied (for some of the earlier work, see [67]). However, the phenomenology of the string-based PV-AMSB model, defined by the soft terms given in (48), has yet to be thoroughly explored. We view this anomaly-dominated regime as a particular limit of string models where supersymmetry is broken by the F-term of some compactification modulus. Note that this anomaly-mediated limit is one in which all tree-level soft supersymmetry breaking terms vanish. We thus choose to begin our study of string-based heterotic orbifold phenomenology at one loop with this particularly simple regime.

Like the minimal AMSB scenario, the PV-AMSB model has two free parameters, apart from $\tan\beta$ and the sign of the μ term. One parameter is the overall scale, given by the gravitino mass $M_{3/2}$. The other parameter is the regularization weight p that determines the size of the scalar mass terms relative to the gaugino masses and A-terms. In this sense, the weight p plays a role comparable to the bulk M_0 postulated in the minimal AMSB scenario, but it is not an ad hoc parameter and it appears elsewhere in the spectrum. Note, however, that the gaugino masses are independent of this weight. Thus, achieving a sufficiently heavy chargino implies a lower bound on the absolute scale as displayed in Fig. 3.

If we look at the branching ratio $b \to s\gamma$, we observe that it becomes important in two situations: small values of the gravitino masses and/or large values of p. As previously mentioned, small gravitino masses give small values of $m_{\chi_1^\pm}$, which leads to a big contribution of the diagram involving $\chi^\pm \tilde{q}$ in the loop for $b \to s\gamma$. Having a large value for p also leads to small squark masses and thus a large contribution from the squark exchange diagrams. Moreover, the same limit $p \to 1$ also leads to light $\tilde{\chi}^0_{3,4}$, $\tilde{\chi}^\pm_2$, which can now also contribute substantially to $b \to s\gamma$ (because of the small μ parameter).

Concerning the Higgs mass, our findings agree with intuition gained from mSUGRA. One needs significant loop contributions from relatively heavy squarks to satisfy the LEP constraint, especially at low $\tan\beta$. Thus re-

[5] The upcoming version of DarkSusy will include these coannihilation channels.

gions where squarks are light are ruled out. This includes the region with $p \to 1$ and smaller gravitino mass scales. In Fig. 3, we show the region excluded by our Higgs mass constraint in the left plot, as well as a contour of $m_{\rm h} = 114\,{\rm GeV}$ for comparison. In the right plot for $\tan\beta = 35$ there is no constraint in this gravitino mass range arising from the Higgs search limit, and we provide contours of $m_{\rm h} = 117\,{\rm GeV}$ and 118 GeV.

With regards to particle observability at the LHC, it is also possible to make some general statements. Here we follow the same guidelines as the authors of [68]. We use masses of 2.5 TeV and lower for gluinos and 1st and 2nd generation squarks to denote possible detectability, which occurs over large portions of the parameter space that we study below. We also indicate regions where the lightest stau has a mass below 200 GeV, where observability will be likely. In all of the allowed parameter space, the lightest neutral Higgs boson will be detectable. Additionally, the lighter neutralinos and charginos are also likely to be detectable. Detectability of individual neutralinos and charginos is a complicated issue depending not only on kinematic accessibility, but also on branching ratios that can vary significantly. Detailed analysis of such individual detectability is beyond the scope of this work. Here we simply point out regions where some neutralinos and charginos are light, lighter than about 250 GeV. So, in this analysis, the main tools of discrimination between the various scenarios comes in detection of the gluino and scalar particles, mainly the lightest stau and the lightest up squark. However, the discovery of the gluino is also quite likely over all scenarios studied here, so its discriminatory value is small. For both plots of Fig. 3, the gluino has a mass below roughly 1 TeV, so it should be easily observable at the LHC. The lightest stau is heavier than roughly 1 TeV in both plots, therefore it is likely to be unobservable. In the right plot, the lightest up squark drops below 2.5 TeV next to the $b \to s\gamma$ constraint line. Within this region (of a width of approximately $\Delta p = 0.2$), 1st and 2nd generation squarks are likely to be observable. The lightest neutralino and chargino are degenerate and their masses are always below 150 GeV in both plots, as can be deduced from the chargino exclusion bound and the dotted line denoting a chargino mass of 130 GeV. The possible detectability of 1st and 2nd generation squarks is the main difference with respect to the LHC between these two plots.

In comparing the two plots, other notable differences come in the mass of the lightest Higgs and also in the importance of the $b \to s\gamma$ constraint. This is a relatively general effect of raising $\tan\beta$ from $\tan\beta = 5$ to $\tan\beta = 35$, and will be seen throughout many of the plots in the remainder of our paper.

In previous AMSB studies it was found that the neutralino thermal relic density is generically too small to explain the amount of dark matter [69]. Due to the low ratio of M_2/M_1 in the AMSB scenarios, the wino content of the LSP is quite high. Additionally, coannihilation between the LSP and the lightest chargino is also very efficient. Both of these effects combine to make the thermal relic density of LSP negligible. Throughout the parameter space of Fig. 3 the thermal relic density is around $\Omega_\chi h^2 \sim 10^{-4}$. Thus, the anomaly-mediated character of the gaugino sector in this model necessitates a non-thermal production mechanism for neutralino LSPs, or another candidate for the cold dark matter must be postulated.

We sum up these constraints in Fig. 4, where we have shown the allowed region in the $(p, \tan\beta)$ plane for a gravitino mass of $M_{3/2} = 40\,{\rm TeV}$. We clearly see that the high $\tan\beta$ area is excluded by $b \to s\gamma$, and the low $\tan\beta$ area is disfavored because of the Higgs mass limit. In every case, p cannot be too large (it must be less than ~ 0.85). This excludes the "minimal" AMSB scenario ($p = 1$) up to the two-loop corrections to soft terms, which have not been fully calculated in these string-based models. Most of the interior of the parameter space in Fig. 4 has sufficiently heavy Higgs masses, as shown by the dashed contours of $m_{\rm h} = 115.5\,{\rm GeV}$ and 117 GeV. The supersymmetric contributions to the $b \to s\gamma$ rate in the interior are small as well. The solid contour is $BR(b \to s\gamma) = 3.53 \times 10^{-4}$. The chargino masses are very light throughout and we have provided contours of $m_{\chi_1^\pm} = 112.5\,{\rm GeV}$ (right-most dotted line) and 113.5 GeV (left-most dotted line). We note that much of this parameter space predicts a relatively small supersymmetric contribution to the muon anomalous magnetic moment due to relatively heavy scalar masses (i.e. $\delta_\mu^{\rm SUSY} \sim 0$). The upper shaded region is ruled out by improper electroweak symmetry breaking ($\mu^2 < 0$). As stated previously, the gluino should be easily detectable at the LHC over the entire allowed parameter space. In this figure, its mass is generally below 800 GeV. Also, the sleptons will be unobservable at the LHC due to their large mass.

In summary, the Pauli–Villars regularization weight p generates a whole class of anomaly-dominated models at the one-loop level. While this new degree of freedom solves the tachyonic slepton problem, the minuscule relic dens-

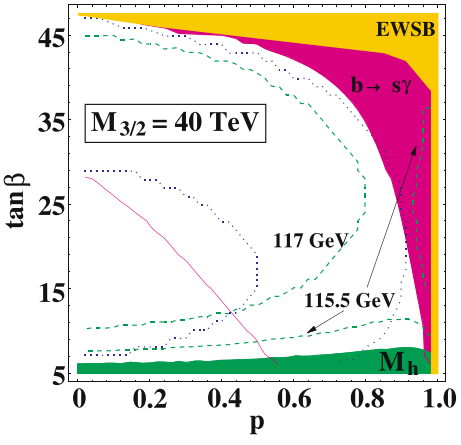

Fig. 4. Constraints on the PV-AMSB parameter space for $M_{3/2} = 40\,{\rm TeV}$. Constraints on the $(p, \tan\beta)$ plane are given for $\mu > 0$. Regions excluded by EWSB failure (*top*), excessive rate for $b \to s\gamma$ (*right*) and the Higgs mass limit (*bottom*) are *shaded*. We have labeled contours of $m_{\rm h} = 115.5$ GeV and 117 GeV (*dashed lines*), as well as unlabeled contours of $m_{\chi_1^\pm} = 112.5$ GeV and 113.5 GeV (*dotted lines*). The *solid contour* in the *lower left* is a contour of $BR(b \to s\gamma) = 3.53 \times 10^{-4}$

ity still does not allow the neutralino to be a thermal dark matter candidate. Additionally, the constraints coming from accelerator physics exclude high values of p and low values of $M_{3/2}$, and predict small contributions to the muon anomalous magnetic moment.

5.3 The general moduli dominated case

We will now relax the assumption that the various Kähler moduli are stabilized at self-dual points, while maintaining the assumption that the modular weights of all matter fields are equal and given by $n_i = -1$. When the vacuum value $\langle \mathrm{Re}\, t \rangle$ is not fixed at $\langle \mathrm{Re}\, t \rangle = 1$, we must use the soft terms in (47). Note that the value of the Green–Schwarz coefficient δ_{GS} becomes relevant for the determination of gaugino masses in this case. For the time being we will take $\delta_{\mathrm{GS}} = 0$ in order to keep the parameter space at a manageable size.

For the study of the moduli dominated case, we have looked at the behavior of the model as a function of the vacuum expectation value (vev) of the real part of the (universal) modulus field $t = T|_{\theta=0}$, for different values of p and $\tan\beta$. To be more precise, we have taken two values of p, 0 and 0.95, and two values of $\tan\beta$, 5 and 35. We have chosen to use the value $p = 0.95$, because at this value the gaugino masses and scalar masses have roughly the same magnitude. It is also very near the pure AMSB limit. We first stress the common features of the moduli-dominated case, and extract the corresponding phenomenological consequences, before looking at specific points in the parameter space.

We choose to investigate the region $0.1 \leq \langle \mathrm{Re}\, t \rangle \leq 5$. Since the vacuum value of this modulus is related to the radius of the compact dimensions, negative values have no physical meaning. Let us note that the combination $(t+\bar{t})G_2(t,\bar{t})$, which appears in the gaugino mass when the equation of motion (11) is substituted into (47), is invariant (up to a sign) under the duality transformation $t \to 1/t$ as shown in Fig. 5. However, since this term competes with the anomaly-mediated contribution to gaugino masses at the one loop level, gaugino masses will not display this duality symmetry. Any value $\langle \mathrm{Re}\, t \rangle \neq 1$ represents a spontaneous breaking of modular invariance and the phenomenology of the theory for $\langle \mathrm{Re}\, t \rangle < 1$ will be different from the case $\langle \mathrm{Re}\, t \rangle > 1$.

Looking again at the gaugino masses in (47), it is clear that when $\delta_{\mathrm{GS}} = 0$, the gaugino masses are proportional to beta-function coefficients. Thus, we expect the phenomenology of this scenario to be very similar to that of the PV-AMSB scenario of the previous section. For example, we continue to have

$$\left.\frac{M_1}{M_2}\right|_{\mathrm{GUT}} = \frac{g_1(\mu_{\mathrm{GUT}})}{g_2(\mu_{\mathrm{GUT}})}\frac{b_1}{b_2} \sim \frac{b_1}{b_2} = \frac{33}{5} = 6.6 \qquad (71)$$

independent of the value of $\langle \mathrm{Re}\, t \rangle$ or p. At the low scale this implies $M_2 \ll M_1$ and the lightest neutralino χ_1^0 and the lightest chargino $\chi_1^\pm$ are in a nearly complete Wino state. This means that for all values of p and $\langle \mathrm{Re}\, t \rangle$, we expect $m_{\chi_1^0} \simeq m_{\chi_1^\pm} \simeq M_2$, and the relic density of the LSP

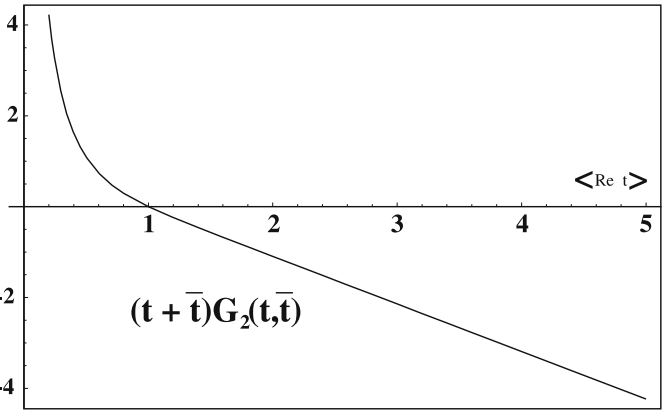

Fig. 5. Behavior of the combination $(t+\bar{t})G_2(t,\bar{t})$ as a function of $\mathrm{Re}\, t$

neutralino is almost entirely depleted by (co)annihilation channels involving χ_1^0 and $\chi_1^\pm$.

Unlike the case of Sect. 5.2, however, there is now a value of $\langle \mathrm{Re}\, t \rangle$, such that the contribution from the Eisenstein function exactly counterbalances the contribution from the superconformal anomaly giving us vanishing gaugino mass soft breaking terms M_a to this order. For the choice of phase conventions in (7) and (8) this occurs when[6]

$$(t+\bar{t})G_2(t,\bar{t}) = 1 \to \zeta(t) = 0 \to \mathrm{Re}\, t = 0.523\,. \quad (72)$$

Not surprisingly, then, we find that much of the parameter space in the vicinity of $\langle \mathrm{Re}\, t \rangle = 0.5$ is ruled out by the chargino mass bounds for any reasonable choice of scale $M_{3/2}$ in Figs. 6 and 7.

In the extreme cases where $\langle \mathrm{Re}\, t \rangle \to 0.1$ and $\langle \mathrm{Re}\, t \rangle \to 5$, the absolute value of the combination $(t+\bar{t})G_2(t,\bar{t})$ becomes large and dominates over the anomaly contribution in the gaugino masses. Here, gauginos will typically be similar in size to the scalar masses at the high scale, particularly as the value of p is increased towards its limiting value $p = 1$ (Fig. 7). The chargino mass bound is easily satisfied here and the increased contribution from M_3 in the RG evolution of the scalar masses makes the Higgs mass constraint easier to satisfy, particularly for large $\tan\beta$. In Fig. 6, we show the Higgs and chargino exclusion regions in the $\tan\beta = 5$ panel, and the contours $m_{\mathrm{h}} = 115\,\mathrm{GeV}$ (dashed line) and $m_{\chi_1^\pm} = 200\,\mathrm{GeV}$ (dotted line). The Higgs mass is not constraining at $\tan\beta = 35$, and we provide contours of $m_{\mathrm{h}} = 115\,\mathrm{GeV}$ and $118\,\mathrm{GeV}$ (dashed lines), and again $m_{\chi_1^\pm} = 200\,\mathrm{GeV}$ (dotted line).

In terms of detectability at the LHC, the $p = 0$ plots in Fig. 6 show some similarity to the anomaly mediated scenario in the previous section. The gluino has a mass that will allow future LHC detection over the bulk of the allowed parameter space. The sleptons are far too heavy for

[6] In [6] the same behavior was noted. In that reference, however, the opposite sign convention on (7) was used, leading to vanishing gaugino masses when $(t+\bar{t})G_2(t,\bar{t}) = -1$, which occurs at the dual point $\mathrm{Re}\, t \simeq 2$.

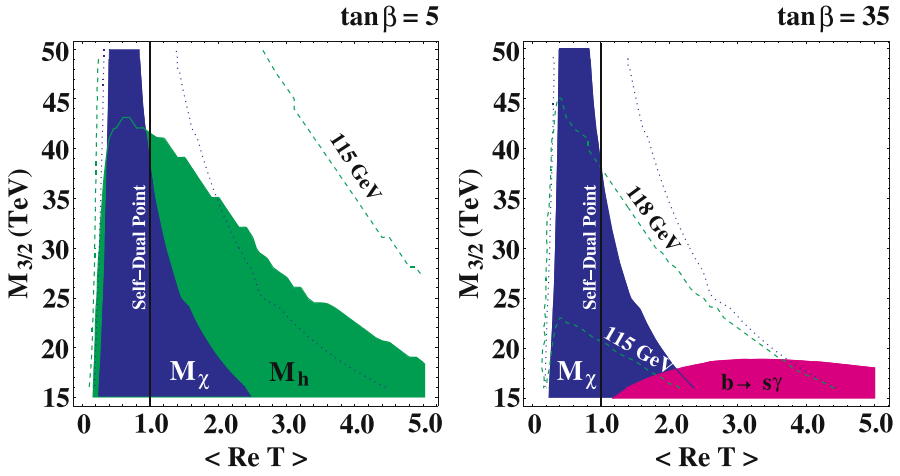

Fig. 6. Constraints on the moduli-dominated parameter space for $\tan\beta = 5$ (*left*) and $\tan\beta = 35$ (*right*) with $p = 0$. Constraints on the $(M_{3/2}, \langle \mathrm{Re}\, t\rangle)$ plane are given for $\delta_{\mathrm{GS}} = 0$ and $\mu > 0$. The region in $\langle \mathrm{Re}\, t\rangle$ shown here is $0.2 \leq \langle \mathrm{Re}\, t\rangle \leq 1$. The areas marked M_χ and M_h are ruled out by the chargino mass bound and the Higgs mass bound, respectively. Chargino masses of $m_{\chi_1^\pm} = 200$ GeV (*dotted line*) are provided in both plots, while Higgs contours of $m_\mathrm{h} = 115$ GeV and 118 GeV (*dashed lines*) are given where applicable

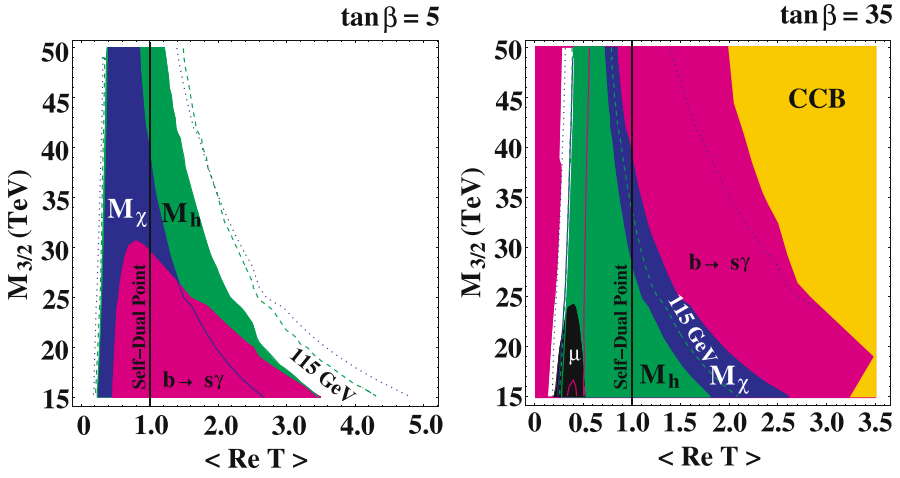

Fig. 7. Constraints on the moduli-dominated parameter space for $\tan\beta = 5$ (*left*) and $\tan\beta = 35$ (*right*) with $p = 0.95$. Constraints on the $(M_{3/2}, \langle \mathrm{Re}\, t\rangle)$ plane are given for $\delta_{\mathrm{GS}} = 0$ and $\mu > 0$. The *shaded region* in the *upper right* of the $\tan\beta = 35$ plot is excluded by CCB constraints, while the *small shaded triangle* in the *lower left* is excluded by improper EWSB. Chargino mass contours of $m_{\chi_1^\pm} = 200$ GeV (*dotted line*) and Higgs mass contours of $m_\mathrm{h} = 115$ GeV (*labeled dashed line*) are given in both plots

detection. Since the lightest neutralino is very degenerate with the lightest chargino, one can see by the dotted line where they both acquire masses of 200 GeV in both plots. Higher masses can be interpolated also using the chargino mass bound.

While the mass contours and exclusion regions in Fig. 6 show the underlying modular symmetry $t \to 1/t$ in a very broad sense, it is clear that these contours do not obey this symmetry in the strict sense. We have indicated the self-dual point $\langle \mathrm{Re}\, t\rangle = 1$ by a heavy vertical line. The exclusion regions do not show the expected duality symmetry about this point. As already mentioned above, this is due in large part to the competition between contributions to the gaugino masses from the moduli sector and contributions from the superconformal anomaly. The relative sign between these contributions depends on which side of the self-dual point the (overall) modulus is stabilized. Having chosen the conventions of (7), (19) and (20), this implies a zero in the gaugino mass formula (30) on a definite side of the self-dual point (with the conventions here, the smaller value side). The conventions can be changed to make this zero occur on the other side, but only at the expense of changing the convention for the sign of the μ parameter. As we keep this sign always fixed at positive values, the relative sign between the gaugino masses — in particular, the gluino mass M_3 — and the μ term is the key variable in distinguishing the two sides of the self-dual point. This is reflected in the fact that at $\tan\beta = 35$ in Fig. 6, the $b \to s\gamma$ constraint applies to only one side of the figure. Other observables, such as the muon anomalous magnetic moment,

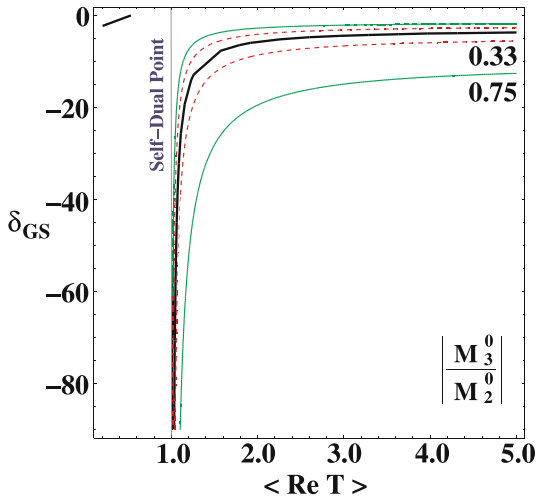

Fig. 8. Contours of relative running gaugino masses M_3/M_2 in the $(\langle \mathrm{Re}\, t\rangle, \delta_{\mathrm{GS}})$ plane. These soft masses are at the initial (GUT) scale. The heavy (*dark*) contour is the limit of vanishing gluino mass (there is another such contour in the *upper left corner* on the other side of the self-dual point). For $\langle \mathrm{Re}\, t\rangle > 1$ we also give contours of $|M_3/M_2| = 0.33$ (*dashed*) and 0.75 (*solid*)

will be sensitive to this relative sign as well, making any spontaneous breaking of modular invariance a true observable, at least in principle.[7]

In comparison with the earlier section, we can see that a heavier lightest Higgs and heavier charginos are possible when $\langle \mathrm{Re}\, t\rangle$ deviates from its self-dual value. As mentioned previously, raising $\tan\beta$ does indeed increase the mass of the lightest Higgs.

As we approach the minimal AMSB limit of $p \to 1$, the relevant constraints change as scalar masses diminish. This is displayed in Fig. 7. The Higgs mass limit is important over much of the parameter space, requiring gravitino mass scales well in excess of 50 TeV for $\langle \mathrm{Re}\, t\rangle \simeq 1$ in order to compensate for the rapidly diminishing stop masses. Note that Figs.6 and 7 correctly reproduce our previous results in the limit of $\langle \mathrm{Re}\, t\rangle \to 1$. The light squarks in the $p \simeq 1$ regime tend to contribute too much to the $b \to s\gamma$ process — a process that provided no such constraint in this region of $\langle \mathrm{Re}\, t\rangle$ in Fig. 6 due to the relatively large scalar masses in those cases.

Nearly the entire region of the parameter space for $\tan\beta = 35$ shown in Fig. 7 is ruled out by this constraint. The remaining slender allowed region near $\langle \mathrm{Re}\, t\rangle \simeq 0.25$ allowed by the experimental constraints is the result of a relatively light charged Higgs that helps to cancel the contributions from the light chargino. Here the scalars and the gauginos are light — in particular, the gluino has a vanishing soft mass at the high scale near $\langle \mathrm{Re}\, t\rangle \simeq 0.3$ when $\delta_{\mathrm{GS}} = 0$ (see Fig. 8). This leads to a very small μ term value in this narrow range, and consequently a small charged Higgs mass. For example, as we move from $\langle \mathrm{Re}\, t\rangle \simeq 0.1$ to $\langle \mathrm{Re}\, t\rangle = 0.3$ along the line $M_{3/2} = 15$ TeV in the right panel of Fig. 6, the value of μ at the electroweak scale drops from 1700 to 1100 GeV due to the diminishing gluino mass. However, in the right panel of Fig. 7 μ goes from 1700 to 380 GeV over the same range, leading to a charged Higgs mass of approximately the same value. Scalar masses are around 200 GeV at this point.

In the right panel of Fig. 7 with $p \to 1$ (light squarks) and large $\tan\beta$ (large couplings in the Higgs sector), there also appears a zone excluded by too large a supersymmetric contribution to the anomalous magnetic moment of the muon (a black region labeled "μ") due to the presence of very light squarks and gauginos. This region is already excluded, however, by multiple observables such as the $b \to s\gamma$ rate, the chargino mass and the Higgs mass bound. The shaded region in the upper right of the $\tan\beta = 35$ plot in Fig. 7 is disfavored by the presence of CCB minima deeper than the preferred electroweak vacuum. The presence of such a region is due to the very large trilinear couplings for these values of $\langle \mathrm{Re}\, t\rangle$, which are larger than the scalar masses when $p \simeq 1$.

With regards to discovery at the LHC, this anomaly-mediated-like scenario with the possibility of being non-self-dual has some unique properties when compared with the earlier sections. Like the previous scenarios, gluino discovery prospects will be excellent except for the upper right hand corner (with $M_{3/2} > 25$ TeV) of each plot. Additionally, the mass of the lightest up squarks is below 2.5 TeV in both plots of Fig. 7, except for the same upper right hand corner. The main unique feature, however, is the possibility of detecting the lightest stau. On the left-hand side of the left plot, the lightest stau mass is quite low, dropping below 200 GeV. At high values of $M_{3/2}$, this only happens right at $\langle \mathrm{Re}\, t\rangle \simeq 0$. However, for gravitino masses below about 25 TeV, such accessible sleptons occur over the entire allowed region to the left of the self-dual line. For $\tan\beta = 35$, the gluino will be accessible in the allowed region, but the lightest stau is not. Again due to the degeneracy of the lightest neutralino and lightest chargino, the dotted line in both plots illustrates when a mass of 200 GeV occurs.

In comparison with Fig. 6, the mass of the lightest Higgs is also in general heavier, except for the region just to the left of the self-dual line for $\tan\beta = 5$. As expected, increasing $\tan\beta$ increases the mass of the lightest Higgs and also the importance of the $b \to s\gamma$ constraint. In this simple moduli-dominated scenario, the phenomenology is similar to that of anomaly mediation. The closer one approaches the minimal AMSB limit of $p = 1$, the more problematic the scenario becomes, particularly at large $\tan\beta$. Other points in the PV-AMSB class have some areas of phenomenological viability, though the chargino and Higgs mass bounds can be quite constraining, particularly near the self-dual point $\langle \mathrm{Re}\, t\rangle = 1$. All of these cases will be unable to explain the cold dark matter content of the universe, at least in terms of thermal relic neutralinos.

Our study of the PV-AMSB scenario of Sect. 5.2 had one effective parameter, the regularization weight p, apart from the overall scale given by the gravitino mass $M_{3/2}$. This regularization weight controls the size of the scalar

[7] For a discussion of these points, in the context of distinguishing anomaly mediation from gauge mediation, see the work of G. Kribs in [67].

mass relative to the fundamental scale $M_{3/2}$, while the gaugino masses were fixed by their beta-function coefficients. In the present section, the parameter space has been expanded to allow for $\langle \mathrm{Re}\, t \rangle \neq 1$, allowing the gaugino masses to be varied relative to the scalars and gravitino mass $M_{3/2}$ in an independent way. Small, or even vanishing, gaugino masses are now possible, as is the possibility of relatively large gaugino masses as one moves far from the self-dual point for the compactification moduli.

Despite this new degree of freedom, the parameter space is still quite constrained. In particular, obtaining the correct relic density for the neutralino LSP is impossible in this framework, because of its extreme wino-like nature. However, as we will see in the next section, the possibility of non-vanishing Green–Schwarz counterterm can open a new region of parameter space completely in accord with present experimental data.

5.4 The influence of the Green–Schwarz counterterm

In this section, we wish to introduce the possibility that $\delta_{\mathrm{GS}} \neq 0$, as would typically be the case in realistic heterotic orbifold constructions. As we will see, this parameter allows one to interpolate between regions with a phenomenology similar to anomaly mediated models (specifically the PV-AMSB scenario of (48)), and regions where the phenomenology resembles that of the minimal supergravity paradigm.

In the conventions defined by the string threshold correction (28), the value of δ_{GS} is a negative integer between 0 and -90. For any given orbifold construction, the precise value of this coefficient can be worked out, and indeed such an exercise has been performed for realistic Z_3 models already [70]. In the figures that follow we will treat this variable as a continuous parameter. At values of the Kähler modulus far from its self-dual point, where the Eisenstein function is not negligible, the term in (47) proportional to δ_{GS} can give rise to substantial (universal) contributions to the gaugino masses. Thus points in parameter space with large values of δ_{GS} and values of $\langle \mathrm{Re}\, t \rangle$ far from unity will be likely to have a pattern of gaugino masses similar to mSUGRA — and hence are more likely to provide a viable dark matter candidate than cases with $\delta_{\mathrm{GS}} \simeq 0$. Furthermore, once $|\delta_{\mathrm{GS}}| \sim \sqrt{16\pi^2} \sim \mathcal{O}(10)$, the gaugino masses and scalar masses will be of approximately the same size. This is very different from the hierarchical situation of the previous sections.

Because of the difference of sign between the beta functions b_a of the standard model gauge groups, M_3 has a particular behavior that differs from the other gaugino masses. This in turn drives the phenomenology of the model, particularly through the gluino's RG effects on the rest of the superpartner spectrum. With a non-vanishing Green–Schwarz coefficient the various gaugino masses will no longer have zeros at the same value of $\mathrm{Re}\, t$. In particular, for certain combinations of $\langle \mathrm{Re}\, t \rangle$ and δ_{GS} it is possible for the gluino mass to vanish at the boundary condition scale while the other gauginos have non-vanishing masses. These combinations are shown in Fig. 8. For parameter choices near these contours we might expect the phenomenologically unacceptable result of a gluino LSP. Even when the gluino is not the LSP, its small value relative to other gauginos may provide too little radiative correction to squark masses and the Higgs mass bound may be difficult to satisfy. On the other hand, a relatively light gluino is likely to reduce the amount of fine-tuning required to obtain $M_Z = 91.2\,\mathrm{GeV}$ [71].

In Figs. 9, 10 and 11 we look at this model in the $(\delta_{\mathrm{GS}}, M_{3/2})$ plane for $p = 0$ and $\langle \mathrm{Re}\, t \rangle = 0.5$, $\langle \mathrm{Re}\, t \rangle = 1.23$ and $\langle \mathrm{Re}\, t \rangle = 2$, respectively. Beginning with the case $\langle \mathrm{Re}\, t \rangle = 0.5$ in Fig. 9, we see that the limit as $\delta_{\mathrm{GS}} \to 0$ reproduces the cases studied in the previous section. In particular, such models require very large $M_{3/2}$ in these regions to satisfy the chargino and Higgs mass constraints. This behavior is seen in all three of the $\langle \mathrm{Re}\, t \rangle$ presented here. A maximum value of $|\delta_{\mathrm{GS}}|$ can, in general, be obtained by requiring that the lightest neutralino be heavier than the lightest stau. For any values of $\tan\beta$, the maximum value of $|\delta_{\mathrm{GS}}|$ is determined by the requirement of keeping the lightest neutralino as the LSP. The quantity $|\delta_{\mathrm{GS}}^{\mathrm{max}}|$ is smaller for higher $\tan\beta$, because the stau is in this case lighter.

In between these disallowed regions, the increasing values of the gaugino masses for fixed scalar mass, as the Green–Schwarz coefficient increases in absolute value, results in smaller contributions to the $b \to s\gamma$ branching ratio and a smaller (in absolute value) anomalous magnetic moment of the muon. In Fig. 9 we have chosen a value of $\langle \mathrm{Re}\, t \rangle$ near the value where gaugino masses vanish when $\delta_{\mathrm{GS}} \to 0$. As is evident from the figure, gaugino masses are indeed falling as this limit is reached. Note that, in this case, there is no point in the plane for which the gluino is the LSP.

Concerning the relic density, it is negligible for small values of the coefficient for the Green–Schwarz counterterm, as we have seen previously: the neutralino is extremely Wino-like in nature and is nearly degenerate with the lightest chargino. Almost all of the relic neutralinos are depleted through coannihilation channels with the charginos. When we increase $|\delta_{\mathrm{GS}}|$, however, we increase the gaugino masses through the increased importance of the $G(t, \bar{t})$ terms in (47). This universal contribution can compete with the (nonuniversal) anomaly-mediated term, driving the gaugino mass terms $M_{i=1,2}$ far away from the previous "degenerate" situation. The gaugino mass sector then begins to look similar to that of mSUGRA and a more bino-like LSP can develop, leading to an increased relic density. Just as in the mSUGRA case, there continues to be a region of stau coannihilation near the excluded stau-LSP area. And — again, just as in mSUGRA — much of the "bulk" area is ruled out by the chargino and Higgs mass bounds, or the $b \to s\gamma$ constraint.

LHC detectability with a non-zero Green–Schwarz term is an especially interesting issue since non-zero δ_{GS} allows the correct value of the neutralino relic density. Over both plots in Fig. 9 the gluino will be, once again, detectable. For $\tan\beta = 5$, there is also a region in the lower left hand corner where the lightest stau has mass below 200 GeV. It is important to note that this region overlaps the region of correct relic density. Similar regions for the

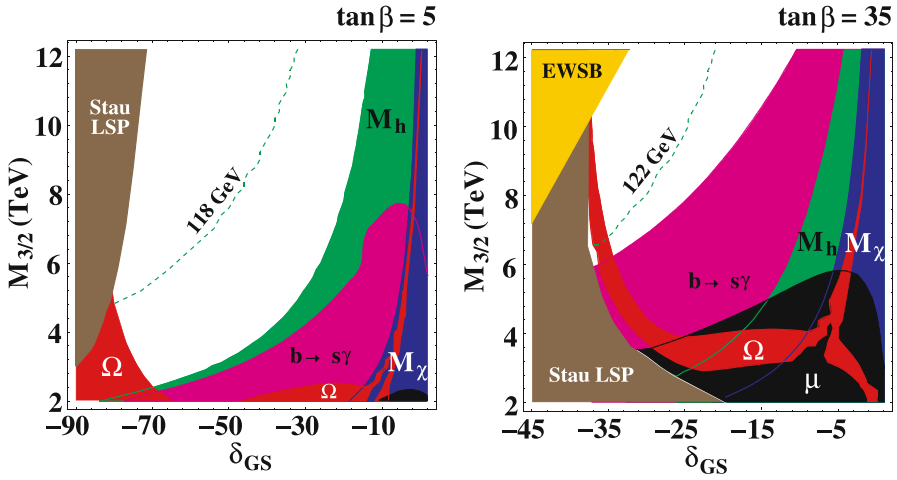

Fig. 9. Constraints on the moduli-dominated parameter space for $\tan\beta = 5$ (*left*) and $\tan\beta = 35$ (*right*) with $p = 0$ and $\langle \mathrm{Re}\, t\rangle = 0.5$. Constraints on the $(M_{3/2}, \delta_{\mathrm{GS}})$ plane are given for $\mu > 0$. *Shaded regions* to the left are ruled out by improper EWSB or a stau LSP. The *dark region* in the *lower right* of the $\tan\beta = 35$ plot labeled "μ" has too much supersymmetric contribution to $(g_\mu - 2)$. The strip labeled "Ω" has the cosmologically preferred neutralino relic density. *Dashed contours* of $m_{\mathrm{h}} = 118$ GeV (*left*) and $m_{\mathrm{h}} = 122$ GeV (*right*) are also given

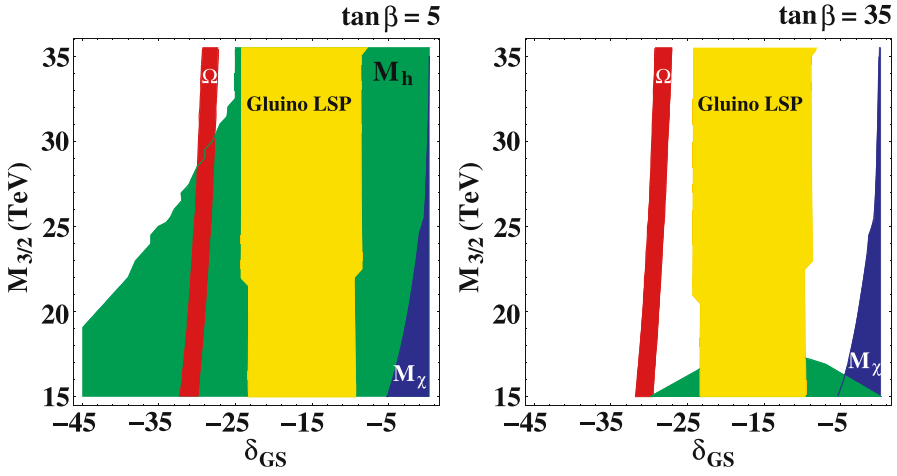

Fig. 10. Constraints on the moduli-dominated parameter space for $\tan\beta = 5$ (*left*) and $\tan\beta = 35$ (*right*) with $p = 0$ and $\langle \mathrm{Re}\, t\rangle = 1.23$. Constraints on the $(M_{3/2}, \delta_{\mathrm{GS}})$ plane are given for $\mu > 0$. The *lightly shaded region* in the center gives a gluino LSP. The *thin strip* with acceptable thermal neutralino relic density is labeled "Ω." Note the change in scale from Fig. 9

stau exist in the right plot, but they are excluded due to the much tighter constraints from $b \to s\gamma$. The lightest up squark has a mass below 2.5 TeV over all of the allowed parameter space, except for the upper left hand corners of both plots with $M_{3/2} > 8$ TeV. In both of these plots, the lightest chargino and neutralino, though no longer degenerate, are both above 250 GeV in all viable areas of parameter space, and so are not likely to be detectable.

It is worth emphasizing that the possibility of having light staus and the correct relic density are two features that scenarios presented here with $\delta_{\mathrm{GS}} = 0$ do not have. It is also worth noting that allowing deviation from $\delta_{\mathrm{GS}} = 0$ tends to increase the mass of the lightest Higgs and the lightest chargino, but tends to decrease the lightest stau mass. Increasing $\tan\beta$ has the same effect as has been commented on before.

In Fig. 10, we investigate the same parameter space for the case where $\langle \mathrm{Re}\, t\rangle = 1.23$. When multiple gaugino condensates are utilized to stabilize the dilaton, with the tree-level Kähler potential given by $K(S, \overline{S}) = -\ln(S + \overline{S})$, a modular invariant treatment of the resulting non-perturbative potential for the moduli fields will lead to the conclusion that the auxiliary field for the dilaton F^S must vanish in the vacuum. The remaining potential for the Kähler moduli leads to their stabilization at this value [72]. Specific points in the space shown in Fig. 10 were singled out for a more detailed study of their collider signatures in a recent set of string-inspired "benchmark" models [73]. Here, a more complete survey of the parameter space is possible.

In accordance with Fig. 8, we note a region centered about $\delta_{\mathrm{GS}} = -15$, where the gluino is the LSP. Interest-

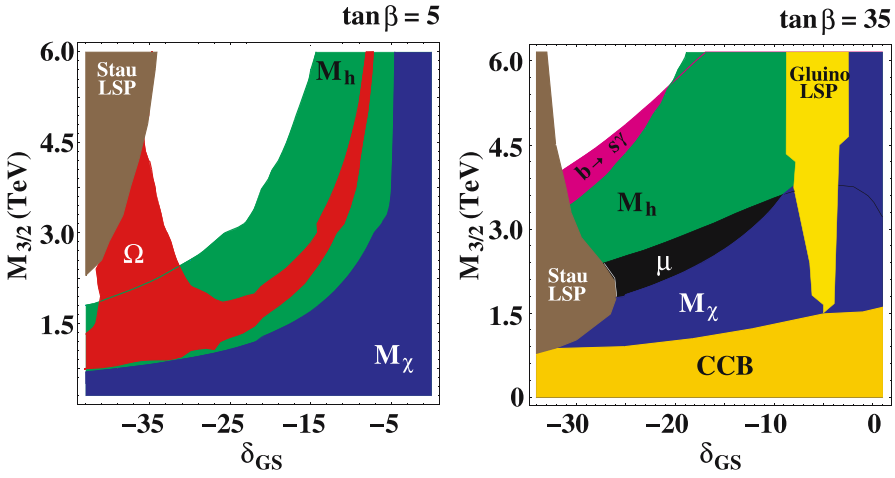

Fig. 11. Constraints on the moduli-dominated parameter space for $\tan\beta = 5$ (*left*) and $\tan\beta = 35$ (*right*) with $p = 0$ and $\langle \mathrm{Re}\, t\rangle = 2.0$. Constraints on the $(M_{3/2}, \delta_{\mathrm{GS}})$ plane are given for $\mu > 0$. The *dark shaded regions* on the left have a stau LSP. The $\tan\beta = 35$ plot also has a region with a gluino LSP. For $\tan\beta = 5$ the region labeled "Ω" has the cosmologically preferred relic density of neutralinos. No such region exists for the higher $\tan\beta$ plot. In that case the exclusion contours are due to (from *bottom right* to *upper left*) CCB vacua, the chargino mass, too large SUSY contributions to $(g_\mu - 2)$, the Higgs mass limit and too large a $b \to s\gamma$ rate

ingly, this is precisely the region of values favored by semi-realistic Z_3 orbifold constructions [70]. To the right, as the absolute value of the Green–Schwarz counterterm diminishes, the chargino mass bound is eventually reached. The value $\langle \mathrm{Re}\, t\rangle = 1.23$ is sufficiently close to the self-dual value that the theory near $\delta_{\mathrm{GS}} = 0$ is anomaly mediated-like in character: very large values of the gravitino mass are generally required to achieve a sufficiently heavy lightest chargino and lightest Higgs (note the difference in scale between Figs. 9 and 10). For $\tan\beta = 35$, the Higgs mass constraint is less important, being only relevant for low gravitino masses near the gluino LSP region. In addition, the LSP is predominantly wino-like on the right side of the gluino LSP region, and the relic density of these neutralinos is negligible.

As we move to larger absolute values of δ_{GS}, we interpolate between this anomaly mediated region and an mSUGRA-like region. For certain critical values of this parameter, the wino content of the LSP is sufficiently reduced to result in the correct annihilation efficiency to produce the cosmologically preferred relic abundance. This change in the character of the LSP is the result of the increasing importance of moduli contributions to the gaugino masses (the first term in the gaugino mass parameter in (47) versus the anomaly mediated contributions (the last term in that expression). The ability to achieve the right relic density, independent of the scalar mass values, is a general property of models with this sort of non-degeneracy among gaugino mass parameters [46, 47].

At the LHC, the detection prospects are quite similar to the earlier models with $\delta_{\mathrm{GS}} = 0$. The gluino will be visible over all allowed parameter space. The lightest stau never becomes light enough to be accessible. In both of these plots, the mass of the lightest up squark is below 2.5 TeV when $M_{3/2}$ drops below 20 TeV. For the right-hand plot, the lightest chargino and neutralino are highly degenerate and are lighter than 250 GeV in all allowed parameter space to the right of the 'gluino LSP' region.

We investigate the case $\langle \mathrm{Re}\, t\rangle = 2.0$ in Fig. 11. The behavior at small $\tan\beta$ is not dissimilar from the nominally "dual" case of $\langle \mathrm{Re}\, t\rangle = 0.5$ in Fig. 9. The stau LSP constraint now arrives at much smaller values of the Green–Schwarz coefficient. Again, the region with the promising relic density of neutralinos is largely constrained by the Higgs mass limit.

Applying the more stringent bounds from WMAP, the cosmologically preferred regions again become thin lines around $\Omega_\chi h^2 = 0.1$. In the left plot of Fig. 9, the only cosmologically preferred region is then the extreme lower left-hand corner. In the right plot of Fig. 9, the edge of the region labeled "Ω" closest to the "Stau LSP" region is still preferred. For both plots in Fig. 10, WMAP singles out the right-hand edge of the "Ω" region closest to the area with a gluino LSP. In Fig. 11, the WMAP-preferred region is along the left-hand edge of the "Ω" region; it runs approximately from the left edge of the plot at $M_{3/2} = 1.35$ TeV up to the "Stau LSP" region at $M_{3/2} = 2.4$ TeV.

The parameter space for the higher $\tan\beta$ regime is even more tightly constrained (at least at these relatively low values of the gravitino mass). We again see a region of gluino LSP — a narrower region at lower absolute values of δ_{GS} consistent with Fig. 8. At the bottom of the plot the values are ruled out by the presence of CCB vacua, while the region to the left has a stau LSP. The light charginos for this value of gravitino mass lead to large contributions to the muon anomalous magnetic moment (the black region labeled "μ"). Finally, all but the uppermost corner of the space is ruled out by the Higgs mass limit and the upper bound on $BR(b \to s\gamma)$.

Now turning our attention towards observability at the LHC, in both plots the gluino and lightest up squark are below 1 TeV over all of the allowed parameter space. In

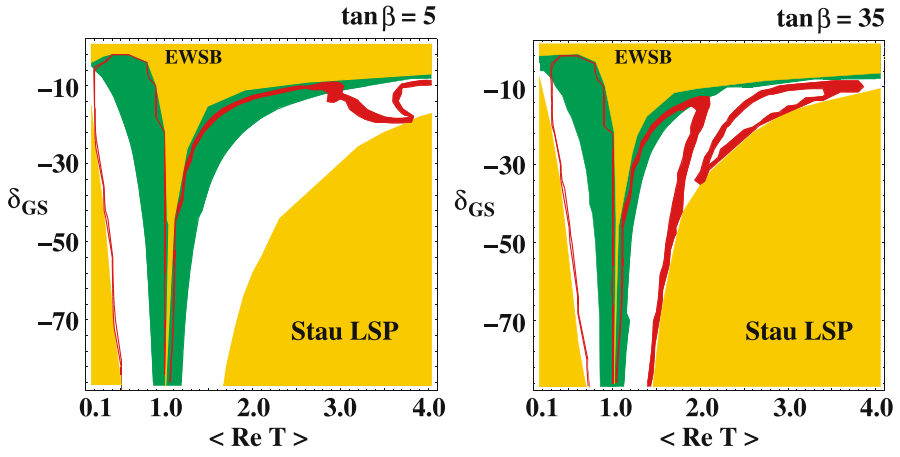

Fig. 12. Constraints on the moduli-dominated parameter space for $\tan\beta = 5$ (*left*) and $\tan\beta = 35$ (*right*) with $p = 0$ and $M_{3/2} = 10$ TeV. Constraints on the $(\langle \mathrm{Re}\, t\rangle, \delta_{\mathrm{GS}})$ plane are given for $\mu > 0$. The *upper light shaded region* has improper EWSB, while the *lower light shaded regions* on either side of $\langle \mathrm{Re}\, t\rangle = 1$ have a stau LSP. All collider constraints have been combined in the *dark shaded region* to make the preferred relic density strip easier to distinguish

addition, the second lightest neutralino is also quite light by LHC observability standards (below 250 GeV) around the 'M_{h}' constraint contour (with a width of approximately $\Delta M_{3/2} = 1$ TeV). The lightest chargino and neutralino will be likely to be detectable in large sections of the parameter space of the left plot. The lightest neutralino is lighter than 250 GeV in all of the allowed parameter space for $\tan\beta = 5$, except for the upper left hand corner starting at $M_{3/2} = 4$ TeV. The chargino, being a little heavier, has a mass below 250 GeV everywhere, except for the upper left hand corner starting at $M_{3/2} = 3$ TeV. For $\tan\beta = 35$, the change in the Higgs and $b \to s\gamma$ constraint has already ruled out all of the parameter space with possibly-detectable lightest neutralinos and charginos.

We combine all of these observational and theoretical constraints to explore the relation between δ_{GS} and $\langle \mathrm{Re}\, t\rangle$ in Fig. 12. We plot the allowed parameter space in the $(\delta_{\mathrm{GS}}, \langle \mathrm{Re}\, t\rangle)$ plane in a similar fashion to Fig. 8 for the specific gravitino mass of $M_{3/2} = 10$ TeV. On either side of the self-dual point at large negative values of δ_{GS}, the stau is the LSP. Near these regions, there is a strip of preferred neutralino relic density. The area at small values of $|\delta_{\mathrm{GS}}|$ and near $\langle \mathrm{Re}\, t\rangle = 1$ is ruled out by improper EWSB. Here, there is again a small strip of preferred relic density, though this is within the region ruled out by the Higgs mass, chargino mass or $b \to s\gamma$ constraint. In the interior there continues to be viable parameter space, including points with acceptable relic neutralino densities. Once again, if we had instead applied the WMAP constraints to the dark matter relic density, the areas would have collapsed to thin strips around $\Omega_\chi h^2 = 0.1$. For the plots in Fig. 12, this area is the edge of the dark shaded region closest to the "EWSB" region.

5.5 The generalized dilaton domination case

If we now consider the other extreme case ($\theta = \pi/2$), the general features are somewhat different. Referring to the soft terms of (52), we can clearly see that the soft scalar mass terms will be roughly dominated by the gravitino mass scale (up to radiative corrections). We anticipate, therefore, that the relevant gravitino mass scale will be approximately one order of magnitude lower than the one necessary in the moduli-dominated case because of the absence of the loop suppression factors on the scalar masses. The gaugino mass soft supersymmetry breaking terms will be determined by the dilaton auxiliary field *vev* $\langle F^S\rangle$.

In the case where nonperturbative corrections to the dilaton Kähler potential are imagined, the minimum of the combined (modular invariant) dilaton/Kähler moduli potential now occurs at $\langle F^S\rangle \neq 0$ and compactification moduli are stabilized at self-dual points where $\langle F^T\rangle = 0$. As described in Sect. 3.2, the requirement of vanishing vacuum energy naturally leads to a suppression of this auxiliary field *vev* relative to the auxiliary field of the supergravity multiplet. Thus, the two contributions to the gaugino mass in (52) each involve a loop suppression factor (unlike the scalar masses) and the dilaton and conformal anomaly contributions are comparable. Indeed, the beta-function coefficients b_a of the standard model gauge groups are of the order of 10^{-2}. Moreover, the F^S term will be driven by b_+, the largest beta-function coefficient among the condensing gauge groups of the hidden sector, from (51) and (49). In fact, if we look in more detail at the expression for F^S in (51), it is apparent that for not too large values of b_+ we can consider that F^S has a linear evolution as a function of that parameter. Increasing b_+ has a direct consequence on the values of the gaugino breaking terms, while increasing $M_{3/2}$ has direct consequences on the general size of all soft breaking terms — in particular soft scalar masses. We can consider the effect of the parameter b_+ as a "fine structure" on top of the gross feature of a hierarchy between scalars and gauginos in this regime.

The general features of this situation are shown in Fig. 13. When the suppression of the gaugino masses is large from small values of b_+ (small a_{np}), the gaugino sec-

tor looks increasingly like that of anomaly-mediation. This is true of any value of $\tan\beta$. As this value is increased, the wino content of the LSP diminishes and we approach the overwhelmingly bino-like LSP of mSUGRA. However, the value of b_+ cannot increase without limit. As we are considering the weakly coupled $E_8 \times E_8$ heterotic string, we cannot imagine a condensing group larger than the complete E_8 of the hidden sector, for which $b_{E_8} = 90/16\pi^2 = 0.57$. It is more likely that the same Wilson-line mechanism that breaks the observable sector gauge group to the product of sub-groups at the compactification scale also breaks the hidden sector group as well. Thus, a more typical range for this parameter might be $b_+ \leq 15/16\pi^2 = 0.095$, where this value corresponds to a pure Yang–Mills sector of $SU(5)$.

For this range of the condensing group beta-function, only small values of $\tan\beta$ are consistent with the stringent demands of electroweak symmetry breaking. This fact was observed in this model some time ago [74], but it is here displayed explicitly in Fig. 13. The large regions marked "EWSB" in this figure have $\bar{\mu}^2 < 0$. This is a manifestation of the "focus point", or hyperbolic nature of this model [65]: the scalar masses are generally much larger than gaugino masses throughout the parameter space. The light gluinos imply that third generation squarks must have large masses at the boundary condition scale to ensure a sufficiently heavy Higgs mass. Thus $M_{3/2} \gtrsim 4$ TeV is needed in the $\tan\beta = 5$ case and $M_{3/2} \gtrsim 1.3$ TeV is needed in the $\tan\beta = 35$ case.

The very large (and nearly universal) scalar masses will imply heavy sleptons at the electroweak scale. Therefore, both direct neutralino annihilation through slepton exchange and $\widetilde{\tau}_1/\chi_1^0$ coannihilation will be ineffective in reducing the relic neutralino density in the early universe. Nevertheless, acceptable relic densities are possible in this model, without the need for resonant annihilation through a heavy Higgs eigenstate. The cosmologically preferred region is the shaded strip labeled "Ω" in Fig. 13. Between this strip and the region ruled out by improper EWSB, the relic density is below the preferred amount. In this region, the LSP has a sufficiently large wino content to annihilate efficiently. Below the marked strip the LSP is bino-like and the relic density is too large. It should be noted again that within the context of heterotic strings on an orbifold, b_+ is limited to $b_+ \leq 0.57$. For both plots in Fig. 13, application of the WMAP result singles out the edge of the "Ω" region closest to the "EWSB" region.

Again with an eye towards LHC prospects, we discover that the dilaton-dominated parameter space looks quite like the moduli-dominated scenario without a Green–Schwarz term: the gluino will be visible, the sleptons will not. However, the lightest neutralino and chargino are both light in the lower left-hand corner of the plot, starting at around $b_+ = 0.2$. Also, the second lightest neutralino is again light in the lower left-hand corner of the left plot, but about 100 GeV heavier than the lightest neutralino. For the right-hand plot, the lightest neutralino has a mass below 250 GeV everywhere, except for the upper right-hand corner of the plot above $M_{3/2} = 3.0$ TeV. The lightest chargino is also light almost everywhere, but not in a region starting at $M_{3/2} = 2$ TeV. The second lightest neutralino and chargino are light over regions similar to the lightest neutralino and chargino, but there masses are approximately 100 GeV heavier than their lighter cousin for a given point in parameter space.

In comparing the dilaton dominated scenario to the earlier sections, we can see that this is only the second option available (other than a non-zero Green–Schwarz term) to achieve the correct relic density. It is also the only scenario studied here that can realize the "focus point" behavior. This is evidenced by the region ruled out by EWSB considerations that exists right next to the region ruled out by the chargino mass limit. As the EWSB region is approached from the allowed region, the value of the μ parameter drops rapidly. First the value drops low enough so that the lightest chargino is mainly higgsino and then becomes ruled out by current experiment. After that, μ^2 eventually drops below zero, signaling improper EWSB. Note, however, that in the dilaton-dominated scenario, no region exists with staus light enough for LHC detection. This is in contrast to what happens when $\delta_{\rm GS}$ deviates from zero.

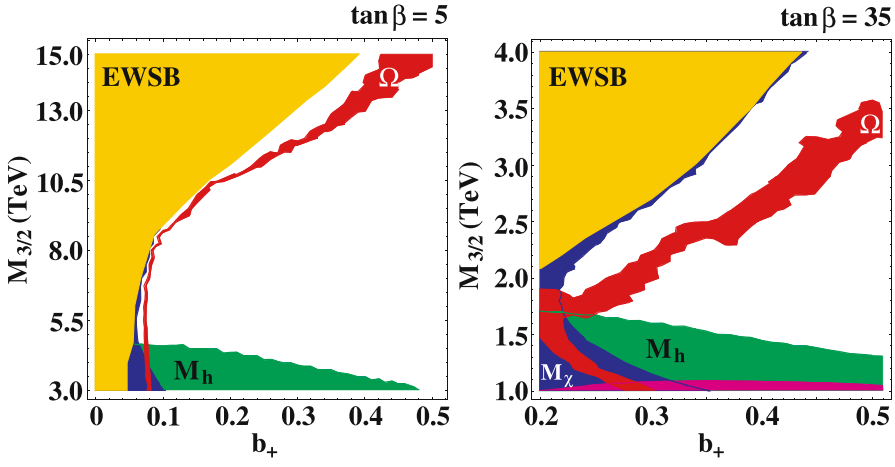

Fig. 13. Constraints on the dilaton-dominated parameter space for $\tan\beta = 5$ (*left*) and $\tan\beta = 35$ (*right*) with. Constraints on the $(M_{3/2}, b_+)$ plane are given for $\mu > 0$

6 Conclusion and perspectives

Even within the restricted context of the weakly-coupled heterotic string compactified on an orbifold, the phenomenology of such supergravity effective theories is far richer and varied than that of the standard "minimal" supergravity approach. While our current indirect knowledge on the nature of supersymmetry already constrains these models significantly, there still exist large regions of parameter space for all the cases studied here — even for low values of $\tan\beta$. We anticipate that future measurements of, or limits on, superpartner masses and kinematic distributions will constrain the parameters of these models further. So too will future cosmological or astrophysical measurements. In fact, these sorts of measurements form a useful complementarity that will be crucial in unraveling the nature of supersymmetry breaking and transmission in such models in the manner begun here. Future studies of string-based models should focus on extending this initial survey to true collider signatures in both hadron and lepton machines, as well as computing event rates for astrophysical processes.

Our analysis in this paper was somewhat cursory — we consider the constraints that arise principally from the chargino and Higgs searches at LEP, as well as the measurement of the branching ratio for $b \to s\gamma$ in the minimal flavor violation scenario. We have indicated, where applicable, the region that seems to be favored by cosmological observations of dark matter relic densities. Interpreting this observation as a constraint on a model implies the assumption that the dark matter is the result of thermal processes in the early universe and is composed entirely of relic neutralino LSPs. In string models many other dark matter candidates are known to exist: axions, superheavy exotic string states, hidden sector gauge and matter condensates, etc., so care should be exercised in applying the cosmological bounds. We have kept the range that we show within the wider region $0.1 \leq \Omega_\chi h^2 \leq 0.3$, though we have commented on the far more restrictive result from the recent WMAP experiment. We have also used only the most conservative possible interpretation of the measurement of the muon anomalous magnetic moment so as to not prematurely prejudice one model versus another.

Furthermore, we have also discussed the possibility of particle detection at LHC. In quite general terms, we find that the lightest neutral Higgs and the gluino will be detectable over almost all of the parameter space allowed by the aforementioned constraints. It is also quite likely that the lighter neutralinos and charginos will be detectable, though more definitive statements go beyond the scope of this paper. In many scenarios, predominantly with higher $\tan\beta$, the lightest up squark is also likely to be observable. We have found that the strongest discriminator between different loop-dominated heterotic orbifold scenarios is the detectability of the lightest stau. We have found that the lightest stau is only light enough to be detectable at the LHC for low values of $\tan\beta$ (around 5). For light staus, it is also required that the compactification moduli be smaller than self-dual ($\langle \mathrm{Re}\, t \rangle < 1$) or that there exist a significant Green–Schwarz term ($\delta_{\mathrm{GS}} < -60$). We thus conclude that within the context of these loop-dominated heterotic orbifold models, detection of the lightest stau at the LHC provides a signature of either spontaneous breaking of modular invariance or a Green–Schwarz counterterm of a size in conflict with explicit calculations of realistic Z_3 orbifold models [70].

Despite the uncertainties that must be borne in mind in such an analysis arising from the computational tools employed (e.g. the choice of quark pole masses utilized, uncertainties in the determination of $\bar{\mu}$ at large $\tan\beta$, etc.), some general statements can certainly be made. Among these is the observation that explicit models of moduli stabilization utilizing field-theoretic methods tend to predict that at least some sector of the theory obtains soft supersymmetry breaking terms only at the one-loop level. This is especially true of the gaugino sector. Furthermore, this suppression leads to the general requirement that the gravitino be relatively heavy in these cases — perhaps alleviating the cosmological problems so often associated with models that contain gravitinos.

A further issue to consider is the importance of parameters relating to the way in which the supergravity theory is regulated. As a non-renormalizable theory we anticipate that the effective supergravity Lagrangian will reflect the UV theory that completes it and cuts off its otherwise divergent behavior at one loop. By choosing to regulate the theory with a manifestly supersymmetric regularization scheme, here using Pauli–Villars superfields, we hope that the regularization can more readily be matched in the future to the underlying string theory at higher genus. The requirements of divergence cancellation and modular invariance preservation highly constrict the nature of these regulating fields, leaving undetermined only the modular weights of fields which generate the supersymmetric PV mass terms. These parameters appear, then, as a kind of stringy threshold correction to the (presumably string-scale) PV masses. This form is consistent with previous calculations of observable quantities at the string one-loop level. If this uncertainty does indeed reflect the underlying physics of massive string modes, then future experiments, by helping to pin down these otherwise free parameters, will be instrumental in probing physics at the string scale.

Apart from these PV-weights, parameters that are related to the orbifold can have a large impact on these broad features. This is a welcome result — implying that experimental data can indeed probe the nature of the underlying theory within a class of models. For example, in cases where supersymmetry breaking is transmitted predominantly by the moduli associated with compactification, the relative sign of terms proportional to their auxiliary field and that of the conformal anomaly can, in principle, be measured. This parameter, in turn, is related to the spontaneous breakdown of modular invariance that may occur in such models.

The phenomenology, even in the simple initial approach taken here, is neither that of minimal supergravity nor minimal anomaly mediation, but is often a hybrid of the two. This makes a detailed study of collider signatures all the more urgent, as search strategies are often based on one or the other of these paradigms. Given that the era of

experimental supersymmetry may well be at hand — and that weakly coupled heterotic strings still represent the best motivated string-based approach to understanding supersymmetry and its breaking in the low-energy world — the time is right for this exciting undertaking.

Acknowledgements. A.B.-H. gratefully acknowledges the hospitality of Laboratoire de Physique Théorique, Université Paris-Sud where significant portions of this work were completed. Y.M. would like to thank E. Dudas and J.B. de Vivie for useful discussions. A.B.-H. is supported in part by the DOE Contract DE-AC03-76SF00098 and in part by the NSF grant PHY-00988-40.

References

1. G.F. Giudice, M. Luty, H. Murayama, R. Rattazzi, JHEP **12**, 027 (1998)
2. L. Randall, R. Sundrum, Nucl. Phys. B **557**, 79 (1999)
3. A. Pomarol, R. Rattazzi, JHEP **05**, 013 (1999)
4. M.K. Gaillard, B.D. Nelson, Y.-Y. Wu, Phys. Lett. B **459**, 549 (1999)
5. M.K. Gaillard, B.D. Nelson, Nucl. Phys. B **588**, 197 (2000)
6. P. Binetruy, M.K. Gaillard, B.D. Nelson, Nucl. Phys. B **604**, 32 (2001)
7. P. Binétruy, M.K. Gaillard, Y.-Y. Wu, Nucl. Phys. B **481**, 109 (1996)
8. P. Binétruy, M.K. Gaillard, Y.-Y. Wu, Nucl. Phys. B **493**, 27 (1997)
9. J.L. Feng, T. Moroi, L. Randall, M. Strassler, S. Su, Phys. Rev. Lett. **83**, 1731 (1999); J.F. Gunion, S. Mrenna, Phys. Rev. D **62**, 015 002 (2000); H. Baer, J.K. Mizukoshi, X. Tata, Phys. Lett. B **488**, 367 (2000); F.E. Paige, J.D. Wells, hep-ph/0001249; A.J. Barr, C.G. Lester, M.A. Parker, B.C. Allanach, P. Richardson, JHEP **03**, 045 (2003)
10. B.C. Allanach, S.F. King, D.A.J. Rayner, JHEP **05**, 067 (2004)
11. U. Chattopadhyay, P. Nath, Phys. Rev. D **70**, 096 009 (2004)
12. A. Brignole, C.E. Ibáñez, C. Muñoz, Nucl. Phys. B **422**, 125 (1994); ERRATUM: Nucl. Phys. B **436**, 747 (1995)
13. L.J. Dixon, V.S. Kaplunovsky, J. Louis, Nucl. Phys. B **355**, 649 (1991)
14. I. Antoniadis, K.S. Narain, T.R. Taylor, Phys. Lett. B **267**, 37 (1991)
15. G.L. Cardoso, B.A. Ovrut , Nucl. Phys. B **369**, 351 (1993)
16. J.-P. Derendinger, S. Ferrara, C. Kounnas, F. Zwirner, Nucl. Phys. B **372**, 145 (1992)
17. M.K. Gaillard, T.R. Taylor, Nucl. Phys. B **381**, 577 (1992)
18. V.S. Kaplunovsky, J. Louis, Nucl. Phys. B **444**, 191 (1995)
19. P. Binétruy, G. Girardi, R. Grimm, Phys. Rept. **343**, 255 (2001)
20. P. Binétruy, M.K. Gaillard, Y.-Y. Wu, Phys. Lett. B **412**, 288 (1997)
21. J. Bagger, T. Moroi, E. Poppitz, JHEP **04**, 009 (2000)
22. B.C. Allanach et al., Eur. Phys. J. C **25**, 113 (2001)
23. R. Rattazzi, A. Strumia, J.D. Wells, Nucl. Phys. B **576**, 3 (2000); I. Jack, D.R.T. Jones, Phys. Lett. B **482**, 167 (2000); M. Carena, K. Huitu, T. Kobayashi, Nucl. Phys. B **592**, 164 (2001)
24. A. Brignole, C.E. Ibáñez, C. Muñoz, C. Scheich, Z. Phys. C **74**, 157 (1997); J.A. Casas, A. Lleyda, C. Muñoz, Phys. Lett. B **380**, 59 (1996); B. de Carlos, G.V. Kraniotis, hep-ph/9610355; S.A. Abel, B.C. Allanach, L.E. Ibáñez, M. Klein, F. Quevedo, JHEP **12**, 026 (2000)
25. T. Banks, M. Dine, Phys. Rev. D **50**, 7454 (1994)
26. J.A. Casas, Phys. Lett. B **384**, 103 (1996)
27. J.A. Casas, Z. Lalak, C. Muñoz, G.G. Ross, Nucl. Phys. B **347**, 243 (1990)
28. B. de Carlos, J.A. Casas, C. Muñoz, Nucl. Phys. B **399**, 623 (1993)
29. S.H. Shenker, In: Random Surfaces and Quantum Gravity, Proc. NATO Adv. Study Institute, Cargese, France, 1990, O. Alvarez, E. Marinari, P. Windey (eds.), NATO ASI Series, (Plenum, New York, 1990)
30. T. Barreiro, B. de Carlos, E.J. Copeland, Phys. Rev. D **57**, 7354 (1998)
31. A. Djouadi, J.L. Kneur, G. Moultaka, hep-ph/0211331, http://www.lpm.univ-montp2.fr:6714/∼kneur/suspect.html
32. G. Gamberini, G. Ridolfi, F. Zwirner, Nucl. Phys. B **331**, 331 (1990)
33. B. de Carlos, J.A. Casas, Phys. Lett. B **309**, 320 (1993)
34. R. Arnowitt, P. Nath, Phys. Rev. D **46**, 3981 (1992)
35. V. Barger, M.S. Berger, P. Ohmann, Phys. Rev. D **49**, 4908 (1994)
36. D. Pierce, J. Bagger, K. Matchev, R. Zhang, Nucl. Phys. B **491**, 3 (1997)
37. G. Belanger, F. Boudjema, A. Pukhov, A. Semenov, Comput. Phys. Commun. **149**, 103 (2002), http://wwwlapp.in2p3.fr/lapth/micromegas
38. LEP Higgs Working Group, LHWG Note/2001-04, hep-ex/0107030
39. ALEPH Collaboration, A. Heister et al. Phys. Lett. B **526**, 191 (2002)
40. ALEPH Collaboration, A. Heister et al. Phys. Lett. B **533**, 223 (2002)
41. ALEPH Collaboration, A. Heister et al. Phys. Lett. B **537**, 5 (2002)
42. For a review, see: E.W. Kolb, M.S. Turner, The Early Universe (Addison-Wesley, New York, 1990)
43. K. Griest, D. Seckel, Phys. Rev. D **43**, 3191 (1991); P. Binetruy, G. Girardi, P. Salati, Nucl. Phys. B **237**, 285 (1984)
44. J.R. Ellis, T. Falk, K.A. Olive, M. Srednicki, Astropart. Phys. **13**, 181 (2000)
45. C. Boehm, A. Djouadi, M. Drees, Phys. Rev. D **62**, 035 012 (2000); J.R. Ellis, K.A. Olive, Y. Santoso, Astropart. Phys. **18**, 395 (2003)
46. A. Birkedal-Hansen, B.D. Nelson, Phys. Rev. D **64**, 015 008 (2001)
47. A. Birkedal-Hansen, B.D. Nelson, Phys. Rev. D **67**, 095 006 (2003)
48. J. Edsjo, P. Gondolo, Phys. Rev. D **56**, 1879 (1997)
49. G. Jungman, M. Kamionkowski, K. Griest, Phys. Rept. **267**, 195 (1996)
50. P. Gondolo, J. Edsjo, L. Bergstrom, P. Ullio, E.A. Baltz, astro-ph/0012234, http://www.physto.se/∼edsjo/darksusy/index.html
51. T. Nihei, L. Roszkowski, R.R. de Austri, JHEP **07**, 024 (2002); T. Nihei, L. Roszkowski, R.R. de Austri, JHEP **03**, 031 (2002); A. Birkedal-Hansen, E. Jeong, JHEP **02**, 047 (2003)
52. J.R. Primack, astro-ph/ 0007187

53. C.L. Bennett et al., Astrophys. J. Suppl. **148**, 1 (2003); WMAP Collaboration, D.N. Spergel et al., Astrophys. J. Suppl. **148**, 175 (2003)
54. H. Baer, C. Balazs, JCAP **0305**, 006 (2003); U. Chattopadhyay, A. Corsetti, P. Nath, Phys. Rev. D **68**, 035 005 (2003); J.R. Ellis, K.A. Olive, Y. Santoso, V.C. Spanos, Phys. Lett. B **565**, 176 (2003)
55. A. Birkedal-Hansen, arXiv:hep-ph/0306144
56. A. Birkedal-Hansen, J.G. Wacker, Phys. Rev. D **69**, 065 022 (2004)
57. S. Bertolini, F. Borzumati, A. Masiero, G. Ridolfi, Nucl. Phys. B **353**, 591 (1991); R. Barbieri, G.F. Giudice, Phys. Lett. B **309**, 86 (1993); F. Borzumati, Z. Phys. C **63**, 291 (1994); F. Borzumati, M. Olechowski, S. Pokorski, Phys. Lett. B **349**, 311 (1995); G. Degrassi, P. Gambino, G.F. Giudice, JHEP **12**, 009 (2000)
58. CLEO Collaboration, M.S. Alam et al., Phys. Rev. Lett. **74**, 2885 (1995); S. Ahmed et al., CLEO CONF 99-10; BELL-CONF-0003, Contribution to the 30th International Conference on High-Energy Physics, Osaka, Japan, 2000
59. Particle Data Group, D.E. Groom et al., Eur. Phys. J. C **15**, 1 (2000), http://pdg.lbl.gov/
60. M. Battaglia, A. De Roeck, J. Ellis, F. Gianotti, K.T. Matchev K.A. Olive, L. Pape, G. Wilson, Eur. Phys. J. C **22**, 535 (2001)
61. S.P. Martin, J.D. Wells, Phys. Rev. D **67**, 015 002 (2003)
62. Muon g-2 Collaboration, H.N. Brown et al., Phys. Rev. Lett. **86**, 2227 (2001); Muon g-2 Collaboration, G.W. Bennett et al., Phys. Rev. Lett. **89**, 101 804 (2002), [Erratum-ibid. **89**, 129 903 (2002)]
63. M. Davier, S. Eidelman, A. Hocker, Z. Zhang, Eur. Phys. J. C **27** (2003) 497; M. Davier, S. Eidelman, A. Hocker, Z. Zhang, Eur. Phys. J. C **31** (2003) 503; M. Davier, Nucl. Phys. Proc. Suppl. **131**, 192 (2004)
64. J.R. Ellis, T. Falk, G. Ganis, K.A. Olive, M. Srednicki, Phys. Lett. B **510**, 236 (2001); J.R. Ellis, K.A. Olive, Y. Santoso, New Jour. Phys. **4**, 32 (2002); L. Roszkowski, R. Ruiz de Austri, T. Nihei, JHEP **08**, 024 (2001); A. Djouadi, M. Drees, J.L. Kneur, JHEP **08**, 055 (2001); H. Baer, C. Balazs, A. Belyaev, JHEP **03**, 042 (2002)
65. K.L. Chan, U. Chattopadhyay, P. Nath, Phys. Rev. D **58**, 096 004 (1998); J.L. Feng, K.T. Matchev, T. Moroi, Phys. Rev. Lett. **84**, 2322 (2000); J.L. Feng, K.T. Matchev, T. Moroi, Phys. Rev. D **61**, 075 005 (2000)
66. B. Allanach, S. Kraml, W. Porod, hep-ph/0302102
67. T. Gherghetta, G. Giudice, J.D. Wells, Nucl. Phys. B **559**, 27 (1999); J.L. Feng, T. Moroi, L. Randall, M. Strassler, S. Su, Phys. Rev. Lett. **83**, 1731 (1999); J. Feng, T. Moroi, Phys. Rev. D **61**, 095 004 J. Gunion, S. Mrenna, Phys. Rev. D **62**, 015 002 G. Kribs, Phys. Rev. D **62**, 015 008 H. Baer, M. Diaz, P. Quintana, X. Tata, Phys. Lett. B **488**, 367 (2000); H. Baer, J.K. Mizukoshi, X. Tata, JHEP **04**, 016 (2000); D.K. Ghosh, A. Kundu, P. Roy, S. Roy, Phys. Rev. D **64**, 115 001 J. Gunion, S. Mrenna, Phys. Rev. D **64**, 075 002 (2001)
68. M. Battaglia, A. De Roeck, J.R. Ellis, F. Gianotti, K.A. Olive, L. Pape, Eur. Phys. J. C **33**, 273 (2004)
69. T. Moroi, L. Randall, Nucl. Phys. B **570**, 455 (2000)
70. J. Giedt, Ann. Phys. **289**, 251 (2001)
71. G.L. Kane, J. Lykken, B.D. Nelson, L. Wang, Phys. Lett. B **551**, 146 (2003)
72. A. Font, L. Ibáñez, D. Lüst, F. Quevedo, Phys. Lett. B **245**, 401 (1990); M. Cvetic, A. Font, L. Ibáñez, D. Lüst, F. Quevedo, Nucl. Phys. B **361**, 194 (1991)
73. G.L. Kane, J. Lykken, S. Mrenna, B.D. Nelson, L. Wang, T.T. Wang, Phys. Rev. D **67**, 045 008 (2003)
74. M.K. Gaillard, B.D. Nelson, Nucl. Phys. B **571**, 3 (2000)